Thin–Walled Structures 216 (2025) 113731

Contents lists available at ScienceDirect

Thin-Walled Structures

journal homepage: www.elsevier.com/locate/tws

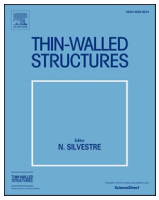

Full length article

On the bending of non-shallow polynomial shells of revolution

Alphose Zingoni [a,*], Nosakhare Enoma [b], Hlasoa Mahlelebe [a]

[a] Department of Civil Engineering, University of Cape Town, South Africa
[b] Department of Mechanical Engineering, University of Benin, Nigeria

ARTICLE INFO

Keywords:
Shell theory
Bending of shells
Shells of revolution
Polynomial shells
Non-shallow shell
Geckeler approximation
Shell slenderness parameter

ABSTRACT

Thin non-shallow polynomial shells of revolution have considerable potential for use as elevated open-top water-retaining structures, and as components of egg-shaped sludge digesters and other large multi-shell liquid-containment concrete structures. However, their structural behaviour as a particular class of thin shells has hardly been studied. Unlike other non-shallow shells of revolution, the slenderness parameter λ of higher-order polynomial shells of revolution generally varies quite rapidly over the edge zone of the shell, which invalidates the use of the popular Geckeler simplification in the evaluation of edge effects. In this paper, we propose, for the first time in the literature, a procedure for the determination of the effective slenderness parameter in the edge zone of such shells, making it possible to take advantage of the Geckeler approximation in the computation of the edge effect, without too much loss of accuracy. The accuracy of the approach is illustrated through consideration of the bending of a parabolic shell of revolution, for which some general parametric results are presented, and actual stresses calculated for the case of a uniformly pressurized shell with fixed edges. Provided the variation of λ does not exceed 30% over the edge zone (which is usually the case), the proposed approach is shown to yield reasonably accurate results (consistent with the errors already inherent in the Geckeler formulation), and is clearly applicable to polynomial shells of higher order.

1. Introduction

Shells of revolution include spherical shells, vertical cylindrical shells, conical shells, ellipsoids of revolution, paraboloids of revolution and toroidal shells, among others. Under axisymmetric loading (such as uniform internal pressure, hydrostatic pressure or self-weight), the deformation response of the shell is also axisymmetric, and various linear-elastic theories have been developed for evaluating the state of stress in such shells under service conditions [1–4]. The membrane theory usually suffices in estimating the state of stress in the shell, provided that: (i) the shell is supported in such a way that the edge of the shell can rotate freely, and the reactions upon the shell coincide with the tangent plane of the shell midsurface; (ii) there are no discontinuities in the shell geometry (shell thickness, meridional slope, meridional radius of curvature, etc.) and loading components (radial and meridional) over the surface of the shell; and (iii) there are no concentrated point loads or line loads on the surface of the shell [3–5]. If these conditions are not met, then resort must be made to the bending theory of shells.

In practice, even if the above conditions are not met, it turns out that for many shells of revolution (particularly those of positive or zero Gaussian curvature), the bending effects are confined to the zones of the shell that are adjacent to the shell supports or interior discontinuities, allowing the membrane solution to be taken as the particular solution of the bending-theory equations, and an edge effect (caused by axisymmetric bending moments and shearing forces) to be taken as the homogenous solution. In such cases, the interior locations of the shell are in a predominantly membrane state of stress (very minimal bending), with only the vicinities of the shell edge and vicinities of interior discontinuities experiencing significant bending stresses. This approach has been used to formulate closed-form solutions for stresses in various applications of shells of revolution [6–10].

In cases where the shell happens to be both relatively thin (i.e. $\frac{t}{r_{min}} < \frac{1}{50}$, where t is the shell thickness, and r_{min} is the minimum radius of curvature of the shell midsurface) and relatively non-shallow (i.e. $\phi_e \geq 45^\circ$, where ϕ_e is the meridional angle of the shell edge), the edge effect will die out from the shell edge (or interior discontinuity) quite rapidly, allowing the Geckeler approximation [1,2,4] to be adopted for the quantification of the edge effect. The Geckeler approximation is most suited to shells that have a constant slenderness parameter λ (such as spherical shells of constant thickness). The parameter λ is primarily a

* Corresponding author.
E-mail address: alphose.zingoni@uct.ac.za (A. Zingoni).

https://doi.org/10.1016/j.tws.2025.113731
Received 8 June 2025; Received in revised form 14 July 2025; Accepted 15 July 2025
Available online 17 July 2025

function of the principal radii of curvature of the shell, r_1 and r_2, and the shell thickness t; it will be defined more precisely in due course. The parameter r_1 denotes the radius of curvature of the shell of revolution in the meridional plane (i.e. the radius of curvature of the shell meridian at the point in question), while r_2 is the radius of curvature of the shell of revolution in the plane perpendicular to the meridional plane *and* containing the normal to the shell midsurface at the point in question); these will be illustrated in due course.

The accuracy of the Geckeler approximation in the computation of bending effects in spherical shells was studied in detail in previous work [11]. This simplified bending theory has been fruitfully applied to the study of bending effects in spherical domes, pressure vessels and liquid-containment vessels [4], for which many useful closed-form results have been obtained. The Geckeler approximation is also capable of giving accurate results in the assessment of bending effects in steep zones of non-shallow shells of revolution of more complex geometry, such as prolate elliptic toroids [10], where the two principal radii of curvature r_1 and r_2 of the shell midsurface (and hence the shell slenderness parameter λ) vary along the shell meridian.

Compared with numerical studies (based on the finite-element method), analytical studies (based on the mathematical theory of shells) have been relatively few over the past 40 years, and these have mainly focused on stress analysis and associated effects. The membrane theory (which is perhaps the simplest version of the theory of shells) has been effectively used to determine the state of stress in domes [12–15], cooling towers [16] and liquid-containment shells [17,18]. It has also been used to determine the membrane state of stress in novel forms of pressure vessels under uniform external pressure, as a first step of a linear buckling analysis of such vessels [19,20]. The more general bending theory of shells (which takes into account both membrane and bending effects) has been applied to the study of stresses around the junctions of conical-shell assemblies [7], multi-segmented spherical shells [6,9], submerged spherical-conical and spherical-parabolic assemblies [21], and elliptic toroids [10,22]. A general review of junction problems in shells has been undertaken by Pietraszkiewicz and Konopinska [23].

Adopting the egg-shaped configuration comprising three spherical-shell segments as first proposed by Zingoni [6], Jiammeepreecha and co-workers have studied the nonlinear static response of such shells under external pressure and using a nonlinear formulation [24], and extended this work to toroidal shells with an egg-shaped cross-section [25]. These investigators have also performed a large-displacement stress analysis (in conjunction with a numerical technique) of a shell of revolution with a meridian described by a fifth-order polynomial function and subjected to hydrostatic pressure [26], and a series of nonlinear static analyses of underwater toroidal shell structures [27,28]. The analytical approach (in conjunction with the finite-element method) has also found application in the study of shells of arbitrary shape (i.e. those other than shells of revolution), one interesting example being the analysis of the hydrostatic response of umbrella-shaped shells deployed as coastal barriers against flooding [29,30].

Studies on the buckling behaviour of shells of revolution have been far more numerous. We will only mention a few here. Godoy and co-workers have investigated the buckling of cylindrical and conical shells used as oil-storage tanks [31–33], while other investigators [34–36] have studied the buckling of thin-walled conical shells under uniform external pressure. As early as 1939, Von Karman and Tsien [37] studied the buckling of spherical shells under uniform external pressure, while more recently, Sato et al. [38] investigated the nonlinear buckling of a complete spherical shell under external pressure and filled with an elastic medium. Toroidal shells have been of particular interest. Sobel and Flügge [39] considered the stability of circular toroidal shells under uniform external pressure, while Jordan [40] studied the buckling response of such shells under hydrostatic pressure. Other investigators have focused on the buckling of elliptic toroidal shells [41–43]. More recently, the buckling behaviour of toroidal shells of other cross-sectional shapes have been investigated [44,45]. Also noteworthy are the buckling studies of Jasion and Magnucki [19,20,46–48], which investigated the behaviour of shell-of-revolution pressure vessels of unusual meridian shapes. Several reviews on various aspects of the buckling of thin shells of revolution are available in the literature; some are general [49], while others are application-specific [50].

Although not as versatile as the finite-element method (FEM), analytical formulations have the merit of yielding closed-form solutions (albeit approximate) that are not only capable of yielding values of stresses more quickly (using no more than a programmable scientific calculator), but are also more amenable to parametric studies that richly inform the preliminary stage of shell design. Closed-form analytical solutions are particularly useful where a large number of cases need to be investigated. They can also serve as valuable benchmarks for checking FEM output.

The present study will focus on the bending of non-shallow thin shells of revolution whose meridian is a polynomial curve with zero slope at the origin (i.e. the pole of the shell of revolution). Owing to their smoothly-varying concave profile whose curvature gradually decreases with increasing arc length from the pole, such polynomial shells of revolution are naturally suited for adoption as deep open-top liquid-containment vessels. For the same diameter of opening at the top, deep polynomial shells of revolution have greater containment capacity than conical vessels of the same height, owing to the upward concavity of their meridian. To the best knowledge of the authors, general polynomial shells of revolution have received relatively little attention in the past, despite their considerable potential in liquid-containment applications (for example, as components of egg-shaped sludge digesters [6], or as elevated high-capacity water reservoirs in confined urban environments [17]. The exception is the parabolic shell of revolution, whose membrane stress behaviour has been the subject of some previous studies [4,17,18]. The authors are not aware of any detailed studies seeking to better understand the bending stress behaviour of general polynomial shells of revolution.

The meridian of the polynomial shell of revolution in the xy Cartesian coordinate system (with the y axis being vertical and coincident with the axis of revolution of the shell, and the x axis being horizontal and passing through the origin) is represented by the equation

$$y = kx^n \tag{1}$$

where k is a constant and n is an integer greater than 1. If $n = 2$, we have a parabolic shell of revolution, if $n = 3$, a cubic shell of revolution, and so forth. Fig. 1 shows a meridian of a polynomial shell of revolution in the xy coordinate system; R denotes the radius of shell at its base (i.e. the maximum value of x), while H denotes the overall height of the shell (i.e. the maximum value of y). Other geometric parameters are as defined in the caption.

If $n \geq 3$, polynomial shells of revolution exhibit certain peculiarities in stress behaviour that are not very well known. For example, and was pointed out in studying the feasibility of various meridian profiles for elevated liquid containment [17], the membrane hypothesis breaks down in the close proximity of the pole (origin of the Cartesian coordinate system) of such shells of revolution, owing to the total loss of curvature there: as $x \to 0$, both r_1 and r_2 tend to infinity (∞), so that the shell becomes locally "flat" (like a plate) and unable to mobilise membrane action. A finite-element stress analysis of the shell using membrane-type elements could fail due to this singularity at the pole, unless techniques are introduced to get around the problem.

At the other extreme, for relatively large values of the vertical coordinate y (corresponding to $y/x \gg 2$), the second principal radius of curvature r_2 tends to the horizontal coordinate x, while r_1 becomes very large; the shell slenderness parameter λ also becomes unusually large and very sensitive to small changes in the meridional angle ϕ, which creates numerical problems in implementing approximate shell-bending formulations such as the Geckeler approximation. In particular, it be-

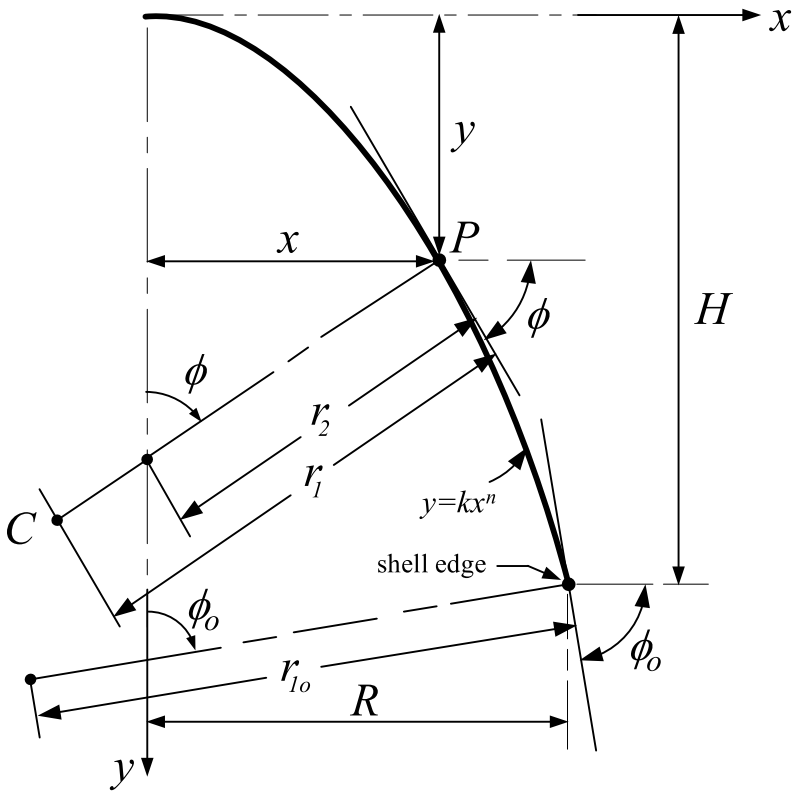

Fig. 1. Geometric parameters of a polynomial shell of revolution: ϕ is the meridional angle at an arbitrary point P on the shell meridian; ϕ_o is the value of ϕ at the edge of the shell; x and y are the Cartesian coordinates at point P; R and H are the values of x and y, respectively, at the edge of the shell; C is the centre of curvature of the meridian at point P; r_1 and r_2 are the principal radii of curvature at point P; r_{1o} is the value of r_1 at the edge of the shell.

comes rather difficult to select an appropriate "average" value of λ to adopt in the edge zone, given the high rate of change of λ with respect to ϕ (the meridional angle coordinate) in the steep zones of polynomial shells of revolution. In these zones where the sides of the shell of revolution are relatively steep ($\phi \geq 75^{\circ}$), the stress behaviour of the polynomial shell of revolution approaches that of a vertical cylindrical shell, and the formulation of the problem may have to be modified accordingly to ensure good accuracy in the assessment of any edge effects there. All these issues have never been investigated before, and it is clear that some guidance for shell practitioners is required.

To complicate matters further, in applying the Geckeler approximation to non-shallow thin shells of revolution where the slenderness parameter λ varies along the shell meridian due to variation of r_1 and r_2 (as in polynomial shells of revolution), there is no guidance in the literature on how the *effective* value of λ (in the zone of the shell experiencing the bending edge effect) should be determined, given that edge effects experience an exponential (and continuous) decay from the edge of the shell into the shell interior, with no clear end point.

In this paper, we propose a logical and consistent procedure for obtaining the effective slenderness parameter in edge zones of non-shallow thin polynomial shells of revolution. The shell slenderness parameter λ is central to the implementation of the Geckeler approximation. Noting that polynomial shells of revolution do not satisfy the assumptions of the Geckeler approximation with regard to the properties of λ, this contribution effectively seeks to "adapt" λ in such a way that the Geckeler approximation can still be used (on account of its simplicity), albeit with diminished accuracy. The procedure is capable of giving results which are sufficiently accurate for most practical applications, but if greater accuracy is required, more iterations of the procedure can be performed. This is the main novelty of this contribution. The applicability of the approach to practical stress analysis is illustrated through consideration of the bending of a non-shallow thin parabolic shell of revolution, for which some general parametric results are presented, and actual stresses calculated for the case of the uniformly pressurized shell with fixed edges.

The structure of the rest of the paper is as follows: In Section 2, the key elements of the Geckeler approximation for axisymmetrically-loaded arbitrary shells of revolution are presented, including expressions for deformations at the edge of the shell and actions in the interior of the shell caused by arbitrary axisymmetric bending and shearing actions applied at the shell edge. Based on compatibility considerations, Section 3 presents general solutions for the edge redundants (the unknowns of the problem) in terms of the edge-effect influence coefficients and membrane-solution edge deformations, for various boundary conditions. In Section 4, the procedure for selecting the effective slenderness parameter of the shell in the edge zone is presented. Section 5 presents useful results for the geometric parameters required for the implementation of the procedure, for both the parabolic and the cubic shell of revolution. In this section (and in the sections that follow), parametric and numerical results are discussed as they are presented (which makes the treatment much easier to follow), *so there is no need for a separate Discussion section*. In Section 6, the procedure is applied to the parabolic shell of revolution, and general closed-form results for the effective slenderness parameter, for various depth-to-radius (H/R) and radius-to-thickness (R/t) ratios of the shell, are calculated and presented. In Section 7, the specific case of a parabolic shell of revolution with fixed edges and subjected to uniform internal pressure is considered, and stresses evaluated for two numerical examples. Analytical results are compared with those generated by finite element modelling, thus validating the proposed procedure. Concluding remarks are made in Section 8.

2. The Geckeler formulation for general shells of revolution

This section summarises the key results of the Geckeler approximation, and provides the theoretical background to the sections that will follow. The Reissner-Meissner equations for the axisymmetric bending

of general shells of revolution are the well-known second-order differential equations in the meridional rotation V and the meridional transverse shear force Q_ϕ [1,2,4]:

$$\left[D\left(\frac{r_2}{r_1}\right)\sin\phi\right]\frac{d^2V}{d\phi^2}+\left[D\left(\frac{r_2}{r_1}\right)\cos\phi+\sin\phi\,\frac{d}{d\phi}\left(D\frac{r_2}{r_1}\right)\right]\frac{dV}{d\phi}$$
$$+\left[\nu\left(\cos\phi\,\frac{dD}{d\phi}-D\sin\phi\right)-D\left(\frac{r_1}{r_2}\right)\frac{\cos^2\phi}{\sin\phi}\right]V=-r_1r_2(\sin\phi)Q_\phi \tag{2a}$$

$$\frac{r_2^2}{tr_1}\frac{d^2Q_\phi}{d\phi^2}+\left[\frac{r_2^2}{tr_1}\cot\phi+\frac{r_2}{tr_1}\frac{dr_2}{d\phi}+\frac{d}{d\phi}\left(\frac{r_2^2}{tr_1}\right)\right]\frac{dQ_\phi}{d\phi}$$
$$+\left[\frac{r_2}{tr_1}\frac{d^2r_2}{d\phi^2}+\left\{\frac{d}{d\phi}\left(\frac{r_2}{tr_1}\right)\right\}\frac{dr_2}{d\phi}+\left\{\left(\frac{r_2+\nu r_1}{r_1}\right)\frac{dr_2}{d\phi}-(r_1+\nu r_2)\cot\phi\right\}\frac{\cot\phi}{t}\right.$$
$$\left.-\nu\left\{(\cot\phi)\frac{d}{d\phi}\left(\frac{r_2}{t}\right)-\left(\frac{r_2}{t}\right)\frac{1}{\sin^2\phi}\right\}\right]Q_\phi=r_1EV \tag{2b}$$

where the geometric parameters r_1, r_2 and t are as already defined, while the material properties E (Young's modulus) and ν (Poisson's ratio) are assumed to be constant throughout the shell; the parameter D is the flexural rigidity of the shell, equal to $Et^3/\{12(1-\nu^2)\}$. If r_1, r_2 and t vary with respect to the meridional angle ϕ (which is the most general situation of a shell of revolution), the coefficients of the differential terms become complicated functions of ϕ, making it extremely difficult to find a general solution for the equations. Fortunately, some simplifications can be made without too much loss in accuracy if the shell is sufficiently thin ($t/r_{min}\leq 1/50$) and non-shallow in the edge zone ($\phi_e \geq 45°$). In such situations, the edge effect decays fairly rapidly with distance from the edge, implying that the second derivatives (with respect to ϕ) of V and Q_ϕ in Eqs. (2) are much larger than the first derivatives, and the first derivatives of V and Q_ϕ are, in turn, much larger than V and Q_ϕ themselves.

Based on the above behaviour, the Geckeler approximation [2,4] (i) neglects the V' and V terms on the left-hand side of Eq. (2a) while retaining only the V'' term, and (ii) neglects the Q' and Q terms on the left-hand side of Eq. (2b) while retaining only the Q'' term (here, the prime and double-prime denote first and second derivatives of a variable with respect to ϕ). This allows the ensuing pair of highly simplified second-order differential equations to be combined into a single fourth-order differential equation in Q_ϕ, the result being [4]:

$$\frac{d^4Q_\phi}{d\phi^4}+\frac{r_1^4Et}{Dr_2^2}Q_\phi=0 \tag{3}$$

that is,

$$\frac{d^4Q_\phi}{d\phi^4}+4\lambda^4Q_\phi=0 \tag{4}$$

where the shell slenderness parameter λ is defined as follows:

$$\lambda=\left\{\frac{r_1^4Et}{4Dr_2^2}\right\}^{1/4}=\left\{3(1-\nu^2)\right\}^{1/4}\frac{r_1}{\{r_2t\}^{1/2}} \tag{5}$$

If, for a given shell, $r_1^4/(r_2^2t^2)$ happens to be constant along a meridian, then λ is constant, and the solution of Eq. (4) is of the same form as that for the spherical shell of constant thickness [2,4]. In general, λ is a function of ϕ, so that an exact solution to Eq. (4) is quite difficult to obtain. Fortunately, owing to the very localized nature of edge effects, λ usually does not vary appreciably over the portion of the shell experiencing significant bending effects, permitting a constant average value for λ to be adopted for the edge zone, and the spherical-shell solution to be applied.

The challenge lies in deciding what constant average value of λ to adopt, since the extent of the bending zone remains unknown until the edge effect has been evaluated, and the evaluation of the edge effect requires λ to be known, a "*catch-22*" situation. In the case of bending effects in equatorial zones of prolate semi-elliptic toroidal shells, we may simply adopt λ_o (the value of λ at the edge of the shell, where $\phi_o=\pm 90°$) as the constant average value of λ; this gives fairly accurate results [10]. However, for non-shallow polynomial shells of revolution represented by Eq. (1), it would not be accurate enough to simply take the value λ at the edge of the shell as the constant average value of λ in the edge zone, given that r_1 varies fairly rapidly with respect to ϕ in the steep zones of the shell experiencing edge effects, which in turn causes λ to vary quite significantly in that zone. A more accurate criterion for the determination of the effective value of λ (i.e. the constant average value of λ that results in the most accurate estimate of edge effects) is required.

A strategy for selecting the best choice of λ for non-shallow polynomial shells of revolution will be presented in Section 4. For now, let us assume such a value of λ has already been determined. Thus, taking λ as a constant (the *effective* value of λ), we may write the solution to Eq. (4) in the form

$$Q_\phi=Ce^{-\lambda\psi}\sin(\lambda\psi+\beta) \tag{6}$$

where C and β are constants of integration, and the coordinate ψ is the angle measured from the shell edge. Denoting the meridional angle corresponding to the shell edge by ϕ_o, the angle ψ is therefore given by $\psi=\phi_o-\phi$ (refer to Fig. 2).

Applying Geckeler-type simplifications to the exact relationships for stress resultants, bending moments and deformations associated with the Reissner-Meissner formulation (refer to standard texts on shell theory [1,2,4] for these), and considering the combined effects of axisymmetric bending moments M_o and horizontal shear forces H_o applied at the edge of the shell as shown in Fig. 3, we finally obtain the following results for internal actions in the shell and deformations at its edge (details of the derivations may be seen in Ref. [4]):

$$N_\phi^b=-\{\cot(\phi_o-\psi)\}\,e^{-\lambda\psi}\left[\frac{2\lambda}{r_1}M_o(\sin\lambda\psi)-H_o(\sin\phi_o)(\sin\lambda\psi-\cos\lambda\psi)\right]$$
$$N_\theta^b=-2\left(\frac{r_2}{r_1}\right)\lambda\,e^{-\lambda\psi}\left[\frac{\lambda}{r_1}M_o(\sin\lambda\psi-\cos\lambda\psi)+H_o(\sin\phi_o)\cos\lambda\psi\right]$$
$$M_\phi=e^{-\lambda\psi}\left[M_o(\sin\lambda\psi+\cos\lambda\psi)-\frac{r_1}{\lambda}H_o(\sin\phi_o)\sin\lambda\psi\right]$$
$$M_\theta=\nu M_\phi \tag{7a-d}$$

$$\left\{\begin{matrix}V_o^b\\ \delta_o^b\end{matrix}\right\}=\left[\begin{matrix}-\frac{4\lambda^3}{Etr_1}\left(\frac{r_2^2}{r_1^2}\right) & \frac{2\lambda^2}{Et}\left(\frac{r_2^2}{r_1^2}\right)\sin\phi_o\\ \frac{2\lambda^2}{Et}\left(\frac{r_2^2}{r_1^2}\right)\sin\phi_o & -\frac{2\lambda}{Et}\left(\frac{r_2^2}{r_1}\right)\sin^2\phi_o\end{matrix}\right]\left\{\begin{matrix}M_o\\ H_o\end{matrix}\right\} \tag{8}$$

Once the redundant edge actions $\{M_o, H_o\}$ have been evaluated (see next section), the interior actions N_ϕ^b, N_θ^b, M_ϕ and M_θ (associated with the edge effect) become known explicitly via the above sets of equations. The total (i.e. net) shell stresses σ_ϕ^T (meridional) and σ_θ^T (hoop) are simply obtained by superimposing membrane stresses with the bending-related edge stresses:

$$\sigma_\phi^T=\frac{N_\phi^m}{t}+\frac{N_\phi^b}{t}\pm\frac{6M_\phi}{t^2}$$
$$\sigma_\theta^T=\frac{N_\theta^m}{t}+\frac{N_\theta^b}{t}\pm\frac{6M_\theta}{t^2} \tag{9a-b}$$

In these expressions, the superscripts m and b associated with the direct stress resultants N_ϕ and N_θ refer to the membrane solution and the bending-related edge effect respectively, while in the double notation $\pm$ associated with bending actions M_ϕ and M_θ, the upper sign refers to the inner surface of the shell, while the lower sign refers to the outer surface.

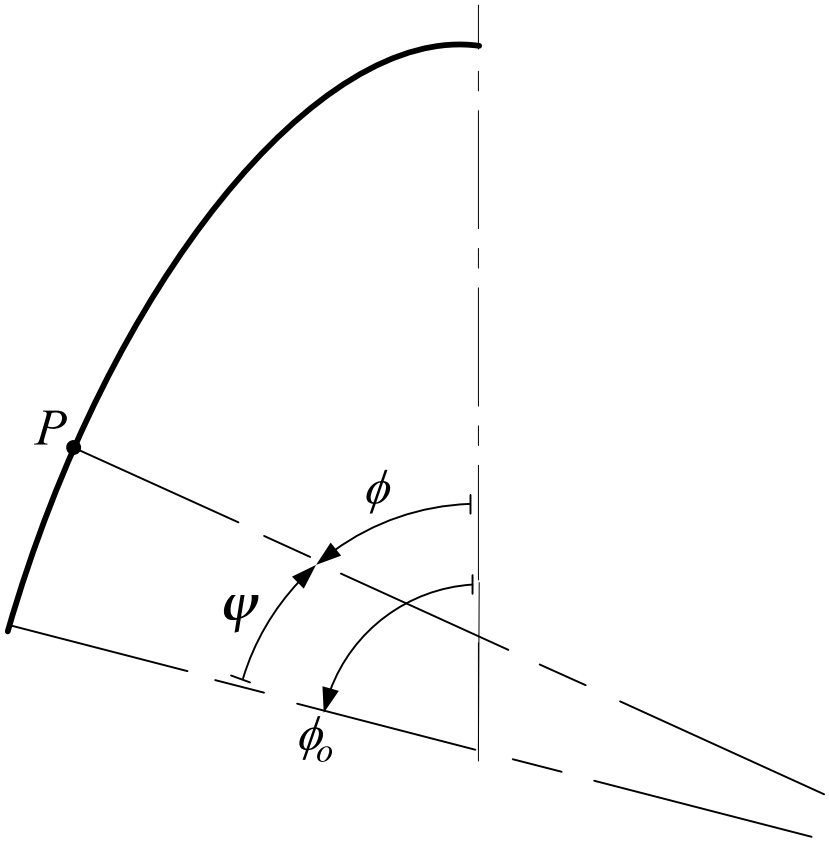

Fig. 2. The relationship between the coordinates ϕ and ψ.

3. General solutions for the edge redundants

The values of the edge actions $\{M_o,\ H_o\}$ to be used in Eqs. (7) depend on the boundary conditions prescribed at the edge of the shell. Some common boundary conditions will be considered in this section, and associated solutions for $\{M_o,\ H_o\}$ presented.

3.1. Flexibility formulation

Eq. (8), relating the bending-related edge deformations to the edge actions $\{M_o,\ H_o\}$ (or *redundants*, by analogy with the compatibility method of structural analysis), may be re-written as

$$\begin{Bmatrix} V_o^b \\ \delta_o^b \end{Bmatrix} = \begin{bmatrix} I_{11} & I_{12} \\ I_{21} & I_{22} \end{bmatrix} \begin{Bmatrix} M_o \\ H_o \end{Bmatrix} \tag{10}$$

where the elements of the square matrix $\{I_{11},\ I_{12},\ I_{21},\ I_{22}\}$ are influence coefficients (or flexibility coefficients) of the shell of revolution, defined as follows:

$$I_{11} = -\frac{4\lambda^3}{Etr_1}\left(\frac{r_2^2}{r_1^2}\right)$$
$$I_{12} = I_{21} = \frac{2\lambda^2}{Et}\left(\frac{r_2^2}{r_1^2}\right)\sin\phi_o \tag{11a-c}$$
$$I_{22} = -\frac{2\lambda}{Et}\left(\frac{r_2^2}{r_1}\right)\sin^2\phi_o$$

3.2. Boundary conditions

Let us consider a shell of revolution with three types of supports, as shown in Fig. 4. These represent situations where (i) both meridional rotation and horizontal translation are restrained (Fig. 4a); (ii) horizontal translation is restrained while meridional rotation is allowed (Fig. 4b); (iii) both meridional rotation and horizontal translation are allowed (Fig. 4c).

3.2.1. Fixed edge

If the edge of the shell is fixed against both rotation and translation (Fig. 4a), we impose the compatibility conditions of zero net meridional rotation of the shell edge ($V_o^T = 0$) and zero net horizontal displacement of the shell edge ($\delta_o^T = 0$), as a way of evaluating the edge redundants M_o and H_o. The net deformations are the result of combining membrane-solution edge deformations and bending-related edge deformations. Thus, we may write

$$\begin{Bmatrix} V_o^T \\ \delta_o^T \end{Bmatrix} = \begin{Bmatrix} V_o^m \\ \delta_o^m \end{Bmatrix} + \begin{Bmatrix} V_o^b \\ \delta_o^b \end{Bmatrix} = \begin{Bmatrix} V_o^m \\ \delta_o^m \end{Bmatrix} + \begin{bmatrix} I_{11} & I_{12} \\ I_{21} & I_{22} \end{bmatrix} \begin{Bmatrix} M_o \\ H_o \end{Bmatrix} = \begin{Bmatrix} 0 \\ 0 \end{Bmatrix} \tag{12}$$

The membrane edge deformations $\{V_o^m,\ \delta_o^m\}$ are assumed to be known quantities (since membrane deformations readily follow once the membrane stress resultants have been evaluated from simple equilibrium considerations of the shell). From the above compatibility conditions, the solutions for the edge redundants $\{M_o,\ H_o\}$ are obtained in closed-form as follows:

$$M_o = \frac{I_{12}\delta_o^m - I_{22}V_o^m}{I_{11}I_{22} - I_{12}^2}$$
$$H_o = \frac{I_{12}V_o^m - I_{11}\delta_o^m}{I_{11}I_{22} - I_{12}^2} \tag{13a-b}$$

recalling that $I_{21} = I_{12}$ (Eq. (11b)).

3.2.2. Fully pinned edge

If the edge of the shell is fully pinned (i.e. free rotation but no

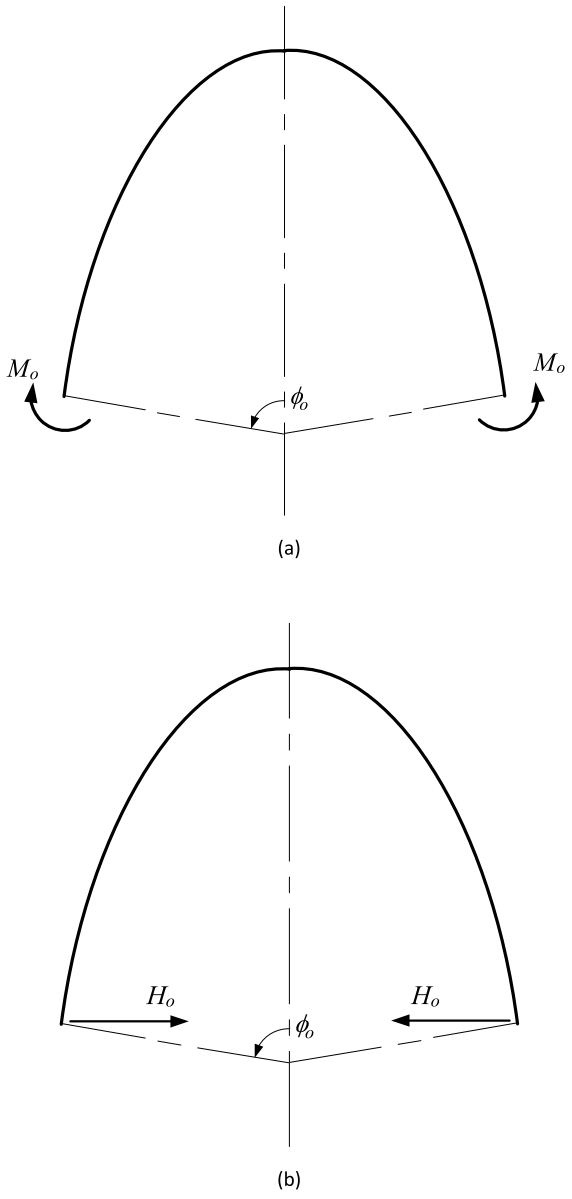

Fig. 3. Axisymmetric bending actions at the edge of the shell: (a) M_o (bending moment per unit length of the shell edge); (b) H_o (horizontal shear force per unit length of the shell edge).

translation allowed (Fig. 4b)), this automatically implies that

$$M_o = 0 \tag{14}$$

Therefore, only H_o is the unknown redundant. We can no longer specify rotation as a boundary condition, but can impose the compatibility condition of zero net horizontal displacement of the shell edge ($\delta_o^T = 0$) as a way of evaluating H_o:

$$\delta_o^T = \delta_o^m + \delta_0^b = \delta_o^m + I_{21}M_o + I_{22}H_o = 0 \tag{15}$$

In the light that $M_o = 0$, we obtain the solution for H_o as follows:

$$H_o = -\frac{\delta_o^m}{I_{22}} \tag{16}$$

3.2.3. Pinned edge on horizontal rollers

If the edge of the shell is pinned on horizontal rollers (Fig. 4c), neither meridional rotation nor horizontal translation can be specified as a boundary condition. Instead, we impose moment equilibrium and

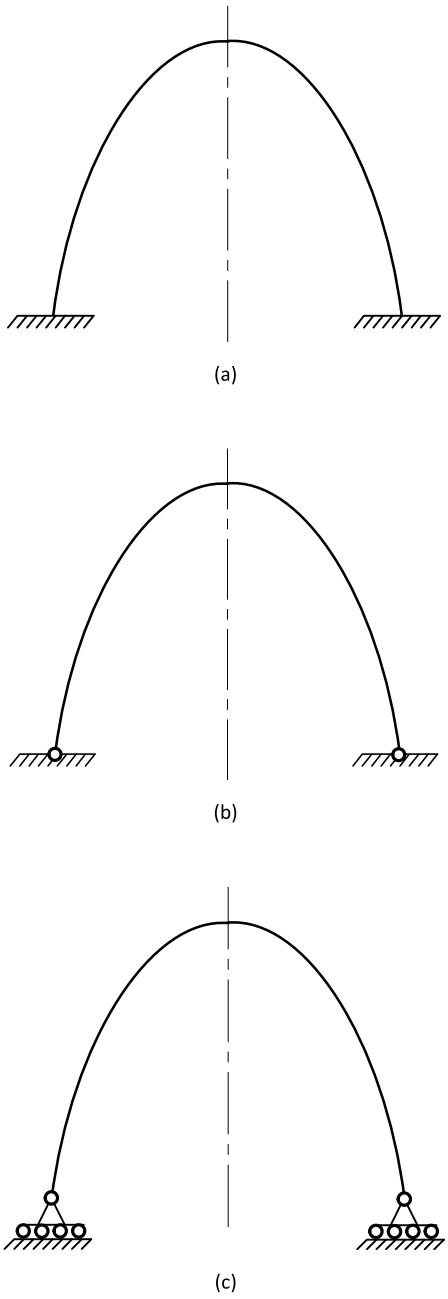

Fig. 4. Shell-edge support conditions: (a) fixed; (b) fully-pinned; (c) pinned on horizontal rollers.

horizontal-force equilibrium to obtain the results:

$$\begin{aligned} M_o &= 0 \\ H_o &= N_o^m \cos\phi_o \end{aligned} \tag{17a-b}$$

where N_o^m is the value of the membrane meridional stress resultant at the shell edge.

4. The effective shell slenderness parameter

In this section, we present a simple yet novel procedure for the determination of the *effective* shell slenderness parameter for shells of revolution whose value of λ varies significantly along the shell meridian, which is the class to which polynomial shells of revolution belong. This approach has never been presented in the literature before, and constitutes the main novelty of this contribution.

From Eq. (7), it is clear that the amplitude of the bending disturbance (as it oscillates while decaying with distance from the edge of the shell) is proportional to $e^{-\lambda\psi}$. We will take the effective range of the bending disturbance (measured from the physical edge of the shell where the redundants M_o and H_o act) as the distance at which the amplitude of the bending disturbance would have decayed to 5% of its initial value. When $\psi = 0$ (at the edge of the shell), the value of $e^{-\lambda\psi}$ is unity. Let ψ_i denote the value of ψ at which $e^{-\lambda\psi}$ becomes 5% of unity. Thus,

$$e^{-\lambda\psi_i} = 0.05 \Rightarrow \lambda\psi_i = 3.00 \Rightarrow \psi_i = \frac{3.00}{\lambda} \text{ (in radians)} \tag{18}$$

Let ϕ_i denote the value of ϕ corresponding to ψ_i. Thus,

$$\phi_i = \phi_o - \psi_i \tag{19}$$

where ϕ_o is, of course, the value of ϕ at the physical edge of the shell. The bounds $\phi = \phi_o$ and $\phi = \phi_i$ (refer to Fig. 5) may be considered as the outer and inner edges of the bending-disturbance zone, within which most of the edge effect occurs. Since λ varies over the edge zone, ψ_i (the angular width of the bending-disturbance zone), and hence ϕ_i (the value of ϕ at the inner edge of the bending-disturbance zone), cannot be determined exactly. An iterative procedure is proposed. The first (or initial) estimates of ψ_i and ϕ_i, denoted by $\psi_{i(1)}$ and $\phi_{i(1)}$ respectively, will be based on the value of the shell slenderness parameter at the physical edge of the shell (i.e. we use λ_o, which is the value of λ at $\phi = \phi_o$). Thus, from Eq. (18), we may write

$$\psi_{i(1)} = \frac{3.00}{\lambda_o} \text{ (in radians)} \tag{20}$$

and from Eq. (19), we may write

$$\phi_{i(1)} = \phi_o - \psi_{i(1)} \tag{21}$$

Based on the value of r_1 (the meridional radius of curvature) at the physical edge of the shell (where $\phi = \phi_o$), and $\psi_{i(1)}$ (the first estimate of the angular width of the bending-disturbance zone), we may estimate the effective range of the bending disturbance as an arc length Δs along the shell meridian, measured from the physical edge of the shell, as follows:

$$\Delta s = r_{1o}\psi_{i(1)} \tag{22}$$

where r_{1o} is the value of r_1 at $\phi = \phi_o$, and $\psi_{i(1)}$ is measured in radians.

Let $\{r_{1o},\ r_{2o}\}$ and $\{r_{1i(1)},\ r_{2i(1)}\}$ denote the values of the principal radii of curvature at the physical edge of the shell (i.e. at $\phi = \phi_o$) and at the inner edge of the bending-disturbance zone as initially estimated (i.e. at $\phi = \phi_{i(1)}$), respectively. Furthermore, let λ_o and $\lambda_{i(1)}$ denote values of the shell slenderness parameter at the outer edge of the bending disturbance zone (i.e. at $\phi = \phi_o$) and at the inner edge of the bending-disturbance zone as initially estimated (i.e. at $\phi = \phi_{i(1)}$), respectively.

Substituting the values of $\{r_{1o},\ r_{2o}\}$ and $\{r_{1i(1)},\ r_{2i(1)}\}$ into Eq. (5), we obtain the expressions for λ_o and $\lambda_{i(1)}$ as follows:

$$\lambda_o = \left\{3\left(1-\nu^2\right)\right\}^{1/4} \frac{r_{1o}}{\{r_{2o}t_o\}^{1/2}}$$
$$\lambda_{i(1)} = \left\{3\left(1-\nu^2\right)\right\}^{1/4} \frac{r_{1i(1)}}{\{r_{2i(1)}t_{i(1)}\}^{1/2}} \tag{23a-b}$$

where t_o and $t_{i(1)}$ are the values of shell thickness at $\phi = \phi_o$ and $\phi = \phi_{i(1)}$ respectively. The *effective* shell slenderness parameter of the first iteration, $\lambda_{e(1)}$, is taken as the average value of λ_o (at the outer edge of the bending zone) and $\lambda_{i(1)}$ (at the inner edge of the bending zone):

$$\lambda_{e(1)} = 0.5(\lambda_o + \lambda_{i(1)}) \tag{24}$$

Eq. (24) gives the value of λ that is proposed for use in the evaluation of the influence coefficients of polynomial shells of revolution (as given by Eqs. (11), with $r_1 = r_{1o}$, $r_2 = r_{2o}$ and $t = t_o$). The effective shell slenderness parameter (as given by Eq. (24)) is also the constant average value of λ that should be used in the evaluation of the internal actions of the edge effect (Eq. (7)).

The first-iteration value of λ (i.e. $\lambda_{e(1)}$) should give sufficient accuracy in most situations (given the very narrow extent of the bending zone), but if greater accuracy is required, a second iteration may be performed. We simply go back to Eq. (18), and recalculate the angular width of the bending zone, but now using the obtained $\lambda_{e(1)}$ instead of λ_o. Denoting

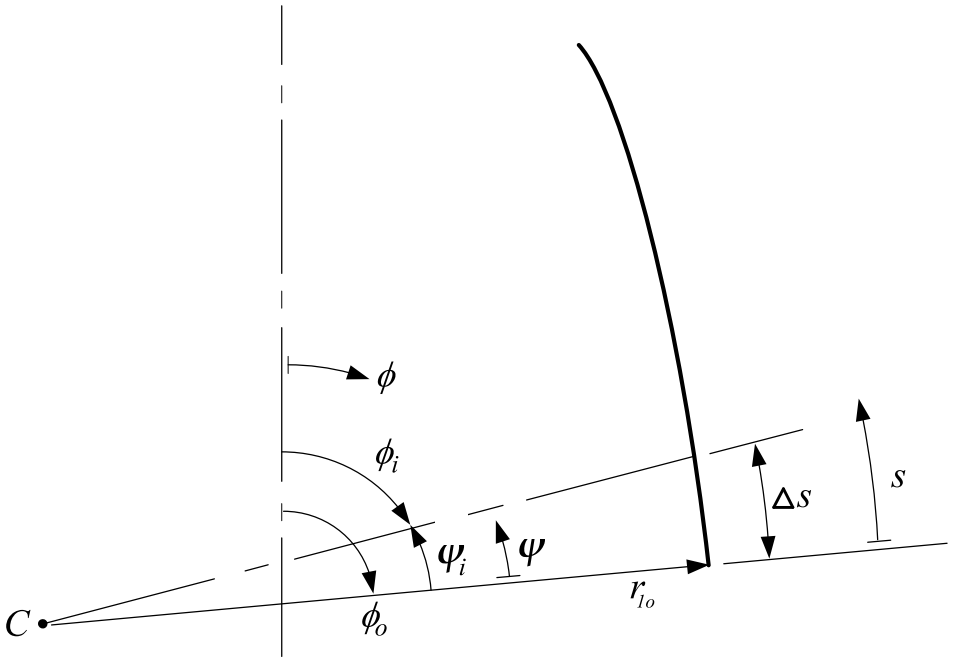

Fig. 5. Parameters of the bending zone: ϕ_i is the value of ϕ at the inner edge of the bending zone (the outer edge being defined by ϕ_o); ψ_i is the value of ψ at the inner edge of the bending zone (the outer edge being defined by $\psi = 0$); s is the arc length from the edge of the shell, measured along the shell meridian; Δs is the effective width of the bending zone.

the angular width of this second iteration by $\psi_{i(2)}$, and the corresponding value of ϕ_i (inner edge of the bending-disturbance zone) by $\phi_{i(2)}$, we may write

$$\psi_{i(2)} = \frac{3.00}{\lambda_{e(1)}} \ \text{(in radians)} \qquad \phi_{i(2)} = \phi_o - \psi_{i(2)} \tag{25a-b}$$

If $\{r_{1i(2)},\ r_{2i(2)}\}$ denote the values of the principal radii of curvature at the inner edge of the bending-disturbance zone as estimated in the second iteration (i.e. at $\phi = \phi_{i(2)}$), then $\lambda_{i(2)}$ (the value of λ at the inner edge of the bending-disturbance zone as estimated in the second iteration) is given by

$$\lambda_{i(2)} = \{3(1-\nu^2)\}^{1/4} \ \frac{r_{1i(2)}}{\{r_{2i(2)} t_{i(2)}\}^{1/2}} \tag{26}$$

where $t_{i(2)}$ is the value of shell thickness at $\phi = \phi_{i(2)}$. The effective shell slenderness parameter of the second iteration, $\lambda_{e(2)}$, is the average value of λ_o at the outer edge of the bending zone and $\lambda_{i(2)}$ at the inner edge of the bending zone:

$$\lambda_{e(2)} = 0.5(\lambda_o + \lambda_{i(2)}) \tag{27}$$

noting that the values of geometric parameters at the outer edge of the bending-disturbance zone (i.e. r_{1o}, r_{2o}, t_o and λ_o) do not change with each iteration. The process may be repeated as many times as is desired (to get increasingly more accurate values of λ_e), but iterations beyond $\lambda_{e(2)}$ are hardly justified. The flowchart in Fig. 6 summarizes the proposed procedure for the calculation of the effective shell slenderness parameter in the bending-disturbance zone of the shell.

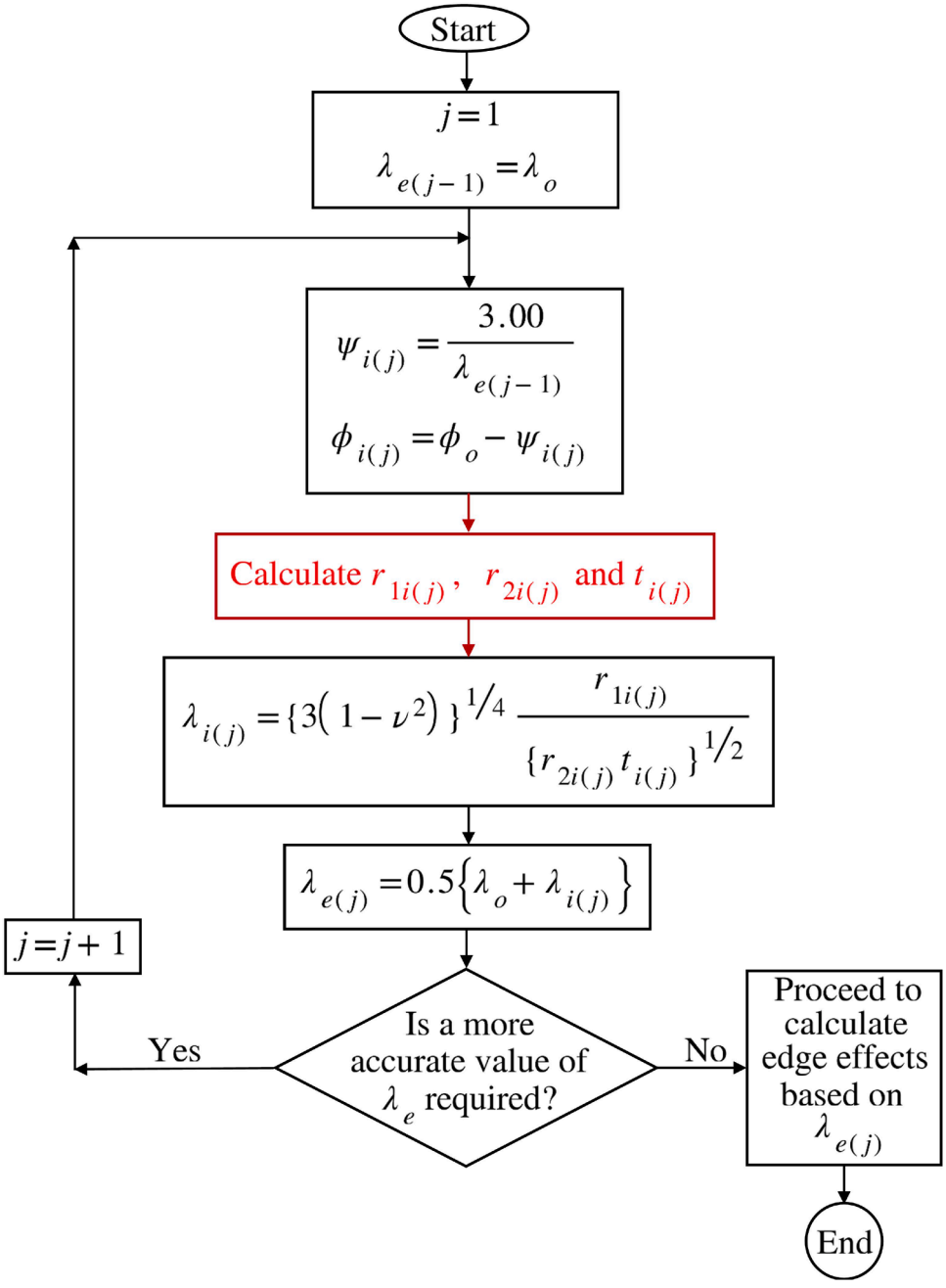

Fig. 6. Flowchart for the calculation of the effective shell slenderness parameter in the bending-disturbance zone of the polynomial shell of revolution.

5. Geometric parameters of polynomial shells of revolution

Let the meridian of a general shell of revolution in the xy coordinate system be described by the function $y = f(x)$ – refer to Fig. 1. By reference to Fig. 1, the slope at a given point P is simply the first derivative of y with respect to x, and this, by definition, is the tangent of the meridional angle ϕ. Thus, the following relationship holds:

$$\frac{dy}{dx} = \tan\phi \Rightarrow \phi = \tan^{-1}\left(\frac{dy}{dx}\right) \tag{28}$$

By reference to the same figure, the second principal radius of curvature may be expressed in terms of the horizontal coordinate x and the meridional angle ϕ as follows:

$$r_2 = \frac{x}{\sin\phi} \tag{29}$$

The first principal radius of curvature is given by the well-known relationship of curve geometry [4]:

$$r_1 = \frac{\left\{1 + \left(\frac{dy}{dx}\right)^2\right\}^{3/2}}{\frac{d^2y}{dx^2}} = \frac{\{1 + \tan^2\phi\}^{3/2}}{\frac{d^2y}{dx^2}} = \left(\frac{1}{\cos^3\phi}\right)\left(\frac{1}{\frac{d^2y}{dx^2}}\right) \tag{30}$$

where use has also been made of the relationship in Eq. (28).

In the case of polynomial shells of revolution of the type represented by Eq. (1), x may be expressed in terms of the tangent of the meridional angle ϕ by making use of the relationship in Eq. (28), allowing the parameters r_1 and r_2 to be in turn expressed in terms of simple trigonometric functions of ϕ. The slenderness parameter λ then follows from Eq. (5). Let us consider two specific cases of polynomial shells of revolution of this type, namely the parabolic shell of revolution, and the cubic shell of revolution. Based on the relationships in Eqs. (28)–(30), and on Eq. (5) for the shell slenderness parameter, the parameters r_1, r_2 and λ are derived as follows:

Parabolic shell of revolution

$$y = kx^2 \tag{31}$$

$$\frac{dy}{dx} = 2kx = \tan\phi \Rightarrow x = \frac{\tan\phi}{2k} \tag{32}$$

$$\frac{d^2y}{dx^2} = 2k \tag{33}$$

$$r_2 = \frac{x}{\sin\phi} = \frac{\tan\phi}{2k\sin\phi} = \frac{1}{2k\cos\phi} \tag{34}$$

$$r_1 = \left(\frac{1}{\cos^3\phi}\right)\left(\frac{1}{\frac{d^2y}{dx^2}}\right) = \frac{1}{2k\cos^3\phi} \tag{35}$$

$$\begin{aligned}\lambda = \{3(1-\nu^2)\}^{1/4}\ \frac{r_1}{\{r_2 t\}^{1/2}} &= \left\{\frac{3(1-\nu^2)}{4}\right\}^{1/4}\left(\frac{1}{\cos^{5/2}\phi}\right)\left(\frac{1}{kt}\right)^{1/2} \\ &= \left\{\frac{3(1-\nu^2)}{4}\right\}^{1/4}\left(\frac{1}{\cos^{5/2}\phi}\right)\left(\frac{1}{Rk}\right)^{1/2}\left(\frac{R}{t}\right)^{1/2}\end{aligned} \tag{36}$$

where R is the base radius of the parabolic shell of revolution (refer to Fig. 1), and R/t is the thinness ratio of the shell relative to the base radius.

Cubic shell of revolution

$$y = kx^3 \tag{37}$$

$$\frac{dy}{dx} = 3kx^2 = \tan\phi \Rightarrow x = \left(\frac{\tan\phi}{3k}\right)^{1/2} \tag{38}$$

$$\frac{d^2y}{dx^2} = 6kx \tag{39}$$

$$r_2 = \frac{x}{\sin\phi} = \left(\frac{1}{3k}\right)^{1/2}\frac{1}{(\sin^{1/2}\phi)(\cos^{1/2}\phi)} \tag{40}$$

$$r_1 = \left(\frac{1}{\cos^3\phi}\right)\left(\frac{1}{\frac{d^2y}{dx^2}}\right) = \frac{1}{6kx\cos^3\phi} = \frac{1}{2}\left(\frac{1}{3k}\right)^{1/2}\frac{1}{(\sin^{1/2}\phi)(\cos^{5/2}\phi)} \tag{41}$$

$$\begin{aligned}\lambda = \{3(1-\nu^2)\}^{1/4}\ \frac{r_1}{\{r_2 t\}^{1/2}} &= \left\{\frac{(1-\nu^2)}{16}\right\}^{1/4}\frac{1}{(\sin^{1/4}\phi)(\cos^{9/4}\phi)}\left(\frac{1}{k}\right)^{1/4}\left(\frac{1}{t}\right)^{1/2} \\ &= \left\{\frac{(1-\nu^2)}{16}\right\}^{1/4}\frac{1}{(\sin^{1/4}\phi)(\cos^{9/4}\phi)}\left(\frac{1}{R^{1/2}k^{1/4}}\right)\left(\frac{R}{t}\right)^{1/2}\end{aligned} \tag{42}$$

where R is the base radius of the cubic shell of revolution (refer to Fig. 1), and as before, R/t is the thinness ratio of the shell relative to the base radius.

As a parametric study, let us consider how the geometric parameters of the shell of revolution vary with its depth ratio $\rho = H/R$ (refer to Fig. 1), based on four values of ρ that cover the full range of non-shallow polynomial shells of revolution, from $\rho = 0.5$ at the lower end, to $\rho = 3.0$ at the higher end. The constant k is evaluated from Eq. (31) (for the parabolic shell of revolution) and Eq. (37) (for the cubic shell of revolution) when x is set to R and y to ρR, which gives $k = \rho/R$ for the parabolic shell, and $k = \rho/R^2$ for the cubic shell of revolution.

The values of the shell parameters at the edge of the shell (when $x = R$ and $\phi = \phi_o$) are of particular interest. To obtain the meridional slope ϕ_o of the parabolic shell of revolution at the base, we substitute $x = R$ and $k = \rho/R$ into Eq. (32), which gives $\phi_o = \tan^{-1}2\rho$. For the cubic shell

Table 1
Geometric parameters of the parabolic shell of revolution for various depth ratios ρ.

$\rho\ (= H/R)$	k	ϕ_o	r_{1o}	r_{2o}
0.5	$0.5/R$	45.000°	$2.828R$	$1.414R$
1.0	$1.0/R$	63.435°	$5.590R$	$1.118R$
2.0	$2.0/R$	75.964°	$17.524R$	$1.031R$
3.0	$3.0/R$	80.538°	$37.514R$	$1.014R$

Table 2
Geometric parameters of the cubic shell of revolution for various depth ratios ρ.

$\rho\ (=H/R)$	k	ϕ_o	r_{1o}	r_{2o}
0.5	$0.5/R^2$	56.310°	$1.953R$	$1.202R$
1.0	$1.0/R^2$	71.565°	$5.270R$	$1.054R$
2.0	$2.0/R^2$	80.538°	$18.757R$	$1.014R$
3.0	$3.0/R^2$	83.660°	$41.255R$	$1.006R$

of revolution, we substitute $x = R$ and $k = \rho/R^2$ into Eq. (38), which gives $\phi_o = \tan^{-1}3\rho$. At the edge of the shell of revolution, the principal radii of curvature, r_{1o} and r_{2o}, are obtained by substituting the applicable values of k and ϕ_o into Eqs. (34) and (35) for the parabolic shell of revolution, and Eqs. (40) and (41) for the cubic shell of revolution. For various depth ratios ρ, Tables 1 and 2 summarise the values of $\{k,\ \phi_o, r_{1o}, r_{2o}\}$ for the parabolic and cubic shells of revolution respectively.

From the above parametric results, we can clearly see the trends in geometric behaviour. As the polynomial shell of revolution becomes deeper, the base angle ϕ_o becomes larger (tends towards 90°) as expected, r_{1o} (the meridional radius of curvature at the base) rapidly increases (large multiples of R), while r_{2o} approaches R more closely. In the lower range of ρ (below $\rho = 1.0$), the r_{1o} values of the parabolic shell are larger than those of the cubic shell, but in the higher range of ρ (above $\rho = 2.0$), the r_{1o} values of the cubic shell become larger than those of the parabolic shell.

The slenderness parameter λ_o (value of λ at the edge of the shell) depends on both the depth ratio ρ (since this dictates the values of k and ϕ_o) and the thinness ratio R/t of the shell – see Eqs. (36) and (42). It also depends on the material property ν (Poisson's ratio). Now, shells of revolution of the polynomial type are most likely to be used when concrete is the constructional material, owing to the ease of mouldability of concrete into any desired shape. Let us therefore assume a Poisson's ratio of $\nu = 0.15$, which is typical of concrete. For various values of depth ratio ρ and thinness ratio R/t, Tables 3 and 4 present values of λ_o for the parabolic and cubic shells of revolution respectively, assuming $\nu = 0.15$. The parametric format of this information makes it particularly useful in preliminary estimates of λ for thin (R/t in the range $50-300$) non-shallow (ρ in the range $0.5-3.0$) parabolic and cubic shells of revolution in concrete.

Comparing Tables 3 and 4, it is worth noting that, for the same depth ratio ρ and thinness ratio R/t, the parabolic shell of revolution has higher values of λ_o than the cubic shell of revolution if $\rho < 1.0$, while the cubic shell of revolution has higher values of λ_o if $\rho > 1.0$. For a given thinness ratio, the two types of shells have approximately the same values of λ_o when $\rho = 1.0$.

From each table, it may be observed that, for a given depth ratio ρ of the shell of revolution, λ_o increases with increasing thinness ratio R/t of the shell, but the rate of increase is slower than that of a linear law (i.e. as the shell becomes thinner, the gain in λ_o per unit increment of R/t becomes smaller). On the other hand, for a given thinness ratio R/t of the shell, λ_o increases quite steeply as the depth ratio ρ is increased, the rate of increase being more rapid than that of a linear law (i.e. as the shell becomes deeper, the gain in λ_o per unit increment of ρ becomes larger). These trends hold for both the parabolic and cubic shells of revolution. We may therefore conclude that while both shell thickness and shell depth have a significant influence on the magnitude of the slenderness parameter λ of polynomial shells of revolution, the influence of shell depth is much greater.

Table 3
Values of λ_o for the parabolic shell of revolution, for various depth ratios ρ and thinness ratios R/t.

	$R/t = 50$	$R/t = 100$	$R/t = 200$	$R/t = 300$
$\rho = 0.5$	22.008	31.124	44.016	53.909
$\rho = 1.0$	48.921	69.185	97.842	119.831
$\rho = 2.0$	159.714	225.870	319.429	391.219
$\rho = 3.0$	344.753	487.550	689.505	844.468

Table 4
Values of λ_o for the cubic shell of revolution, for various depth ratios ρ and thinness ratios R/t.

	$R/t = 50$	$R/t = 100$	$R/t = 200$	$R/t = 300$
$\rho = 0.5$	16.484	23.313	32.969	40.379
$\rho = 1.0$	47.501	67.176	95.002	116.353
$\rho = 2.0$	172.375	243.775	344.750	422.230
$\rho = 3.0$	380.575	538.214	761.149	932.214

To have a better "feel" for these numbers, let us compare them with those for spherical shells of radius a and constant shell thickness t. For such spherical shells, the value of λ (which is constant along the meridian for a given shell) varies from about 7.0 to 22.0 for concrete shells in the range $a/t = 30\rightarrow300$, and from about 22.0 to 32.0 for steel shells in the range $a/t = 300\rightarrow600$. On the other hand, polynomial shells of revolution of comparable thinness are characterised by much higher values of λ. For instance, while a spherical concrete shell with $a/t = 300$ has a λ value of only 22.0, a parabolic concrete shell of revolution with $R/t = 300$ has a λ value at the support which varies from 53.909 when $\rho = 0.5$ to as high as 844.468 when $\rho = 3.0$; a cubic concrete shell of revolution with $R/t = 300$ has a λ value at the support which varies from 40.379 when $\rho = 0.5$ to as high as 932.214 when $\rho = 3.0$.

The half-wavelength of the bending-disturbance sinusoidal oscillations – refer to Eqs. (6) and (7) – is given by $\lambda\psi = \pi$, which gives $\psi = \pi/\lambda$ (in radians) or $\psi = 180°/\lambda$. This means ψ is very small if λ is very large. For example, when $\lambda = 932.214$ (the λ_o value of the cubic shell of revolution for the case $\rho = 3.0$ and $R/t = 300$), we get $\psi \approx 0.19°$, a very small angle indeed. Thus, in numerical computations, in order to accurately capture the stress response in such a narrow edge zone, very small increments of the angle ψ have to be adopted. Since a change in arc length Δs in the edge zone is given $\Delta s = r_1(\Delta\psi)$, and given that the meridional radius r_1 is very large in the edge zone of deep polynomial shells of revolution, it is recommended that the variation of stresses in the edge zone of deep polynomial shells of revolution be plotted versus arc length s from the edge of the shell (where $\phi = \phi_o$), rather than the meridional angle ψ from the shell edge.

6. Application to the parabolic shell of revolution

In this section, the procedure for the determination of the effective shell slenderness parameter λ_e, as proposed in Section 4, is applied to the parabolic shell of revolution, using the results for geometric parameters as presented in Section 5. Only one iteration ($j = 1$) will be performed in the implementation of the procedure illustrated in Fig. 6. The computational stages are set out in tabular format for each of the four parametric cases of depth ratio, namely $\rho = 0.5$ (Table 5), $\rho = 1.0$ (Table 6), $\rho = 2.0$ (Table 7) and $\rho = 3.0$ (Table 8).

Although the parameter λ_o for all 16 combinations of ρ and R/t was given in Table 3, it has been included in Tables 5–8 in order to serve as a starting point for the sequence of calculations leading to the first estimate $\lambda_{e(1)}$ of the effective slenderness parameter for each row. The meridional-angle parameters $\psi_{i(1)}$ and $\phi_{i(1)}$, corresponding to the inner extent of the bending-disturbance zone, are calculated from Eqs. (20)

Table 5
Computation of the effective slenderness parameter for the parabolic shell of revolution for $\rho = 0.5$.

R/t	λ_o	$\psi_{i(1)}$	$\phi_{i(1)}$	Δs	$\lambda_{i(1)}$	$\lambda_{e(1)}$	Var(λ)
50	22.008	7.810°	37.190°	$0.385d$	16.336	19.172	26%
100	31.124	5.523°	39.477°	$0.273d$	25.002	28.063	20%
200	44.016	3.905°	41.095°	$0.193d$	37.536	40.776	15%
300	53.909	3.188°	41.812°	$0.157d$	47.260	50.585	12%

Table 6
Computation of the effective slenderness parameter for the parabolic shell of revolution for $\rho = 1.0$.

R/t	λ_o	$\psi_{i(1)}$	$\phi_{i(1)}$	Δs	$\lambda_{i(1)}$	$\lambda_{e(1)}$	Var(λ)
50	48.921	3.514°	59.921°	0.343d	36.793	42.857	25%
100	69.185	2.484°	60.951°	0.242d	56.324	62.755	19%
200	97.842	1.757°	61.678°	0.171d	84.409	91.126	14%
300	119.831	1.434°	62.001°	0.140d	106.137	112.984	11%

Table 7
Computation of the effective slenderness parameter for the parabolic shell of revolution for $\rho = 2.0$.

R/t	λ_o	$\psi_{i(1)}$	$\phi_{i(1)}$	Δs	$\lambda_{i(1)}$	$\lambda_{e(1)}$	Var(λ)
50	159.714	1.076°	74.888°	0.329d	133.316	146.515	16.5%
100	225.870	0.761°	75.203°	0.233d	198.494	212.182	12.1%
200	319.429	0.538°	75.426°	0.165d	291.332	305.381	8.8%
300	391.219	0.439°	75.525°	0.134d	362.806	377.013	7.3%

Table 8
Computation of the effective slenderness parameter for the parabolic shell of revolution for $\rho = 3.0$.

R/t	λ_o	$\psi_{i(1)}$	$\phi_{i(1)}$	Δs	$\lambda_{i(1)}$	$\lambda_{e(1)}$	Var(λ)
50	344.753	0.499°	80.039°	0.326d	303.559	324.156	12%
100	487.550	0.353°	80.185°	0.231d	445.620	466.590	8.6%
200	689.505	0.249°	80.289°	0.163d	646.545	668.025	6.2%
300	844.468	0.204°	80.334°	0.133d	801.830	823.150	5.0%

and (21), while Δs (the arc-length distance from the edge of the shell to the inner extent of the bending-disturbance zone) is estimated on the basis of Eq. (22). The parameter $\lambda_{i(1)}$ (the shell slenderness parameter at the inner edge of the bending-disturbance zone) is calculated from Eq. (36) with the meridional angle ϕ set equal to $\phi_{i(1)}$. The effective slenderness parameter, $\lambda_{e(1)}$, is finally evaluated from Eq. (24).

An indication of the magnitude of the variability of λ over the bending-disturbance zone is given by the parameter Var(λ) in the last column, calculated as the relative difference between the λ values at the outer and inner edges of the bending-disturbance zone, as follows:

$$\text{Var}(\lambda) = \left[\frac{\lambda_o - \lambda_{i(1)}}{\lambda_o}\right] \times 100\% \tag{43}$$

From the above results, we note that the variability of λ over the bending-disturbance zone, as measured by the parameter Var(λ), decreases with increasing R/t for a constant depth ratio ρ of the shell, which means that as the shell becomes thinner, the difference between λ_o (the value of λ at the support) and λ_e (the more refined value of λ as given by the procedure of Section 4) becomes smaller. For a constant thinness ratio R/t of the shell, the variability of λ over the bending-disturbance zone also decreases with increasing depth ratio ρ, meaning that as the shell becomes deeper, the difference between λ_o and λ_e becomes smaller.

Based on the above observations, we may recommend that, for parabolic shells of revolution of constant thickness, λ_o (the value of λ at the support) may be adopted for the purposes of estimating the edge effect based on the Geckeler approximation, if the shell is both relatively thin and relatively non-shallow (i.e. if $\rho \geq 2.0$ and $R/t \geq 200$, or if $\rho \geq 3.0$ and $R/t \geq 100$).

Table 9
Non-dimensional values of influence coefficients for the parabolic shell of revolution for $\rho = 0.5$.

R/t	$\lambda_{e(1)}$	$I_{11}Et^2$	$I_{12}Et$	$I_{22}E$
50	19.172	− 49.836	129.97	− 677.8
100	28.063	− 78.147	278.471	− 1 984.4
200	40.776	− 119.866	587.924	− 5 766.6
300	50.585	− 152.565	904.807	− 10 730.7

Table 10
Non-dimensional values of influence coefficients for the parabolic shell of revolution for $\rho = 1.0$.

R/t	$\lambda_{e(1)}$	$I_{11}Et^2$	$I_{12}Et$	$I_{22}E$
50	42.857	− 45.059	131.42	− 766.65
100	62.755	− 70.735	281.79	− 2245.19
200	91.126	− 108.289	594.178	− 6 520.43
300	112.984	− 137.600	913.410	− 12 126.69

Table 11
Non-dimensional values of influence coefficients for the parabolic shell of revolution for $\rho = 2.0$.

R/t	$\lambda_{e(1)}$	$I_{11}Et^2$	$I_{12}Et$	$I_{22}E$
50	146.515	− 49.679	144.113	− 836.110
100	212.182	− 75.443	302.243	− 2 421.697
200	305.381	− 112.458	626.070	− 6 970.810
300	377.013	− 141.073	954.226	− 12 908.887

Table 12
Non-dimensional values of influence coefficients for the parabolic shell of revolution for $\rho = 3.0$.

R/t	$\lambda_{e(1)}$	$I_{11}Et^2$	$I_{12}Et$	$I_{22}E$
50	324.156	− 53.051	151.400	− 864.150
100	466.590	− 79.106	313.682	− 2 487.713
200	668.025	− 116.079	642.990	− 7 123.404
300	823.150	− 144.784	976.285	− 13 166.342

Let us also evaluate the influence coefficients I_{11}, $I_{12}(= I_{21})$ and I_{22} for various combinations of shell depth ratios ρ and shell thinness R/t. The influence coefficients are evaluated on the basis of Eqs. (11), using the effective shell slenderness parameter λ_e over the bending-disturbance zone, and the values of r_1, r_2 and ϕ at the edge of the shell. Thus, in Eqs. (11), we simply replace the parameter λ with the value of $\lambda_{e(1)}$ for the combination of ρ and R/t in question (as read from Tables 5–8), the parameters $\{r_1,\ r_2\}$ with the values of $\{r_{1o},\ r_{2o}\}$ for the

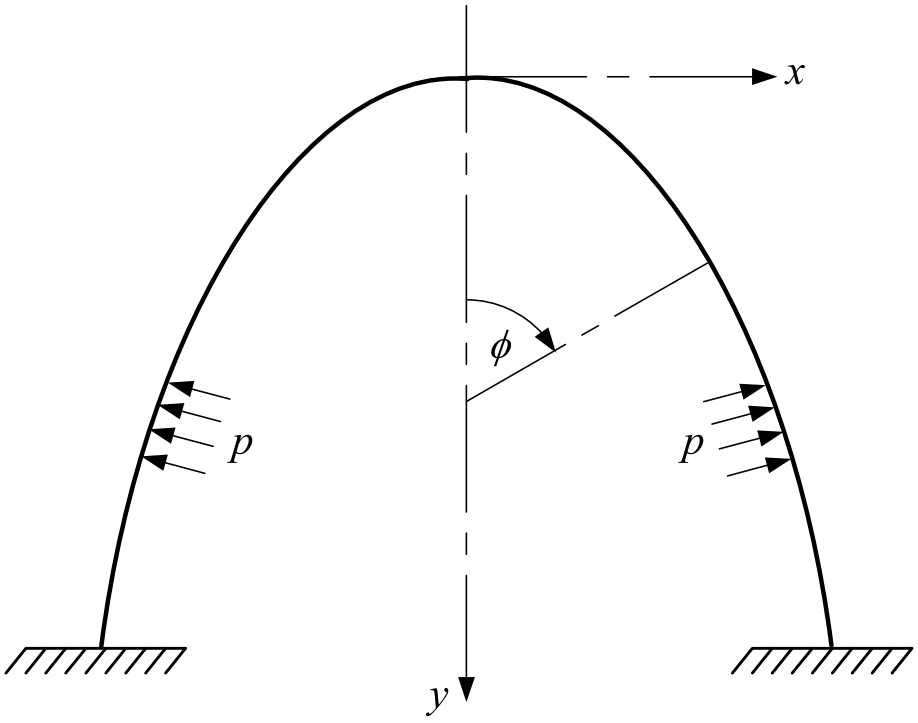

Fig. 7. Numerical example: shell of revolution with a fixed edge and subjected to uniform internal pressure p.

ρ in question (as read from Table 1), and the parameter ϕ_o with the applicable value as given in Table 1. Non-dimensional results for I_{11}, $I_{12}(=I_{21})$ and I_{22} are given in Tables 9–12.

7. Numerical results and validation

7.1. Membrane stress resultants and edge deformations for uniform pressure loading

Let us consider a parabolic shell of revolution whose meridian is described by Eq. (31). The shell is fixed at the base, and subjected to a uniform internal pressure p as illustrated in Fig. 7. The membrane stress resultants in shells of revolution subjected to axisymmetric surface loading, namely N_ϕ^m (in the meridional direction) and N_θ^m (in the hoop direction), are given by the well-known equilibrium-based relationships [4]:

$$N_\phi^m = \frac{1}{r_2 \sin^2\phi}\int \{r_1 r_2 (p_r \cos\phi - p_\phi \sin\phi)\sin\phi\} d\phi + \beta$$
$$N_\theta^m = r_2 p_r - \frac{r_2}{r_1} N_\phi^m \qquad \text{(44a-b)}$$

where p_r and p_ϕ are loading components in the radial direction (i.e. normal to the shell midsurface) and the meridional direction (i.e. tangential to the shell meridian) respectively, and β is a constant of integration. Substituting into the first of Eqs. (44) the geometric parameters r_1 and r_2 as given by Eqs. (34) and (35), and the values of the loading components for uniform internal pressure (namely, $p_r = p; p_\phi = 0$), we obtain an expression for N_ϕ^m which may easily be integrated, and the constant β evaluated from the condition of finiteness of N_ϕ^m at the top of the shell [4]. With N_ϕ^m thus known, the hoop stress resultant N_θ^m follows from the second of Eqs. (44). The results are surprisingly simple (noting that ϕ may be written as $(\phi_o - \psi)$):

$$N_\phi^m = \frac{p}{4k}\left(\frac{1}{\cos\phi}\right) = \frac{p}{4k}\left(\frac{1}{\cos(\phi_o - \psi)}\right)$$
$$N_\theta^m = \frac{p}{4k}\left(\frac{1}{\cos\phi}\right)(2 - \cos^2\phi) = \frac{p}{4k}\left(\frac{1}{\cos(\phi_o - \psi)}\right)(2 - \cos^2(\phi_o - \psi)) \qquad \text{(45a-b)}$$

The membrane deformations of interest are δ^m (the horizontal displacement at a given point) and V^m (the rotation of the shell meridian at a given point). For shells of revolution subjected to axisymmetric surface loading, the following general relationships hold [4]:

$$\delta^m = \frac{1}{Et}(r_2 \sin\phi)\left(N_\theta^m - \nu N_\phi^m\right)$$
$$V^m = \frac{1}{r_1}\left[\frac{\cot\phi}{Et}\left\{(r_1 + \nu r_2)N_\phi^m - (r_2 + \nu r_1)N_\theta^m\right\} - \frac{d}{d\phi}\left\{\frac{r_2}{Et}\left(N_\theta^m - \nu N_\phi^m\right)\right\}\right] \qquad \text{(46a-b)}$$

Substituting into these expressions the solutions for N_ϕ^m and N_θ^m as given by Eqs. (45), we obtain the results:

$$\delta^m = \frac{p}{8k^2 Et}\left(\frac{\sin\phi}{\cos^2\phi}\right)\{2 - (\nu + \cos^2\phi)\}$$
$$V^m = \frac{p}{4kEt}\left[\frac{1}{\sin\phi}\{1 - 2\nu - 2(1-\nu)\cos^2\phi + \cos^4\phi\} - 2(2-\nu)\sin\phi\right] \qquad \text{(47a-b)}$$

It is the edge deformations, δ_o^m and V_o^m, that are required in the computation of the edge effect. These are given by replacing ϕ with ϕ_o in the above relations, as follows:

$$\delta_o^m = \frac{p}{8k^2 Et}\left(\frac{\sin\phi_o}{\cos^2\phi_o}\right)\{2 - (\nu + \cos^2\phi_o)\}$$
$$V_o^m = \frac{p}{4kEt}\left[\frac{1}{\sin\phi_o}\{1 - 2\nu - 2(1-\nu)\cos^2\phi_o + \cos^4\phi_o\} - 2(2-\nu)\sin\phi_o\right] \qquad \text{(48a-b)}$$

7.2. Numerical example

A parabolic shell of revolution with fixed edges has the following numerical values of geometric, material and loading parameters:

$R = 10$ m

$t = 0.1$ m (constant)

$E = 28 \times 10^9$ N/m^2

$\nu = 0.15$

$p = 10\,000$ N/m^2 (internal pressure)

It is required to evaluate the net shell stresses in two cases of depth ratio:

(a) Case 1: $\rho\left(=\frac{H}{R}\right) = 1.0$

(b) Case 2: $\rho\left(=\frac{H}{R}\right) = 2.0$

From the given data, it is noted that the thinness ratio has the value: $R/t = 100$

Step 1. Determine the shell parameters ϕ_o and k

For Case 1, Table 1 gives: $\phi_o = 63.435^\circ$; $k = \frac{1.0}{R} = \frac{1}{10\text{m}} = 0.1$ m^{-1}

For Case 2, Table 1 gives $\phi_o = 75.964^\circ$; $k = \frac{2.0}{R} = \frac{2.0}{10\text{m}} = 0.2$ m^{-1}

Step 2. Evaluate the influence coefficients I_{11}, I_{12} and I_{22}

The influence coefficients I_{11}, $I_{12}(=I_{21})$ and I_{22} are evaluated from Table 10 (for Case 1) and Table 11 (for Case 2), using the row for $R/t = 100$, and the given numerical values of E and t. The results are:

Case 1:

$I_{11} = -2.52625 \times 10^{-7}$ N^{-1}

$I_{12} = I_{21} = +1.00639 \times 10^{-7}$ mN^{-1}

$I_{22} = -8.01854 \times 10^{-8}$ m^{2}N^{-1}

Case 2:

$I_{11} = -2.69439 \times 10^{-7}$ N^{-1}

$I_{12} = I_{21} = +1.07944 \times 10^{-7}$ mN^{-1}

$I_{22} = -8.64892 \times 10^{-8}$ m^{2}N^{-1}

Step 3. Evaluate the shell edge redundants M_o and H_o

The shell edges are fixed, so we use the closed-form solutions for $\{M_o,\ H_o\}$ given by Eqs. (13), with the influence coefficients $\{I_{11},\ I_{12},\ I_{22}\}$ being the values yielded by Step 2, and the membrane edge deformations $\{\delta_o^m,\ V_o^m\}$ being the values yielded by Eqs. (48) using the given data and the $\{\phi_o, k\}$ values in Step 1. The results for $\{\delta_o^m,\ V_o^m\}$, then $\{M_o,\ H_o\}$, are as follows:

Case 1:

$\delta_o^m = +3.29422 \times 10^{-4}$ m

$V_o^m = -2.55551 \times 10^{-5}$

$M_o = 3\,070.888$ Nm/m

$H_o = 7\,962.478$ N/m

Case 2:

$\delta_o^m = +3.29709 \times 10^{-4}$ m

$V_o^m = -1.32477 \times 10^{-5}$

$M_o = 2\,956.161$ Nm/m

$H_o = 7\,501.614$ N/m

Step 4. Evaluate principal radii of curvature r_1 and r_2 at interior locations

The values of r_1 and r_2 at interior locations of the shell defined by the angle ϕ are given by Eqs. (34) and (35). After substituting the value of k for Case 1 and Case 2 as given in Step 1, Eqs. (34) and (35) may be written in terms of the angle ψ (measured from the shell edge):

Case 1: $r_1 = \frac{5\text{ m}}{\cos^3\phi} = \frac{5\text{ m}}{\cos^3(\phi_o-\psi)}$; $r_2 = \frac{5\text{ m}}{\cos\phi} = \frac{5\text{ m}}{\cos(\phi_o-\psi)}$ where $\phi_o = 63.435^\circ$

Case 2: $r_1 = \frac{2.5\text{ m}}{\cos^3\phi} = \frac{2.5\text{ m}}{\cos^3(\phi_o-\psi)}$; $r_2 = \frac{2.5\text{ m}}{\cos\phi} = \frac{2.5\text{ m}}{\cos(\phi_o-\psi)}$ where $\phi_o = 75.964^\circ$

Step 5. Evaluate bending-related actions at interior locations

On the basis of Eqs. (7), the four internal actions $N_\phi^b,\ N_\theta^b,\ M_\phi$ and M_θ associated with the edge effect are next evaluated at various points defined by the coordinate ψ. This is performed by substituting: (i) in place of λ, the effective slenderness parameter $\lambda_e = 62.755$ for Case 1 (as given by Table 6 for $R/t = 100$) and $\lambda_e = 212.182$ for Case 2 (as given by Table 7 for $R/t = 100$); (ii) the M_o and H_o values as calculated in Step 3; (iii) the r_1 and r_2 values as calculated in Step 4; (iv) the value of ϕ_o for the case in question (as given in Step 1).

Step 6. Evaluate the membrane actions at interior locations

Membrane actions at interior locations of the shell are evaluated from Eqs. (45) using the given value of p, and the values of k and ϕ_o for the case in question (as given in Step 1).

Step 7. Evaluate the net stresses at interior locations

The net stresses on the inner and outer surfaces of the shell are finally evaluated from Eqs. (9), completing the stress analysis of the shell.

For Cases 1 and 2, Figs. 8 and 9 show meridional and hoop total-stress variations for the inner and outer surfaces of the shell. Analytical results, calculated on the basis of Steps 1 to 7, are shown on the left, while the results of a finite-element analysis, generated by the FEM programme ABAQUS using the 3-node quadratic axisymmetric thin shell element (SAX2), are shown on the right. This shell element has three degrees of freedom at each node, namely translations in the x and y directions, and meridional rotation in the xy plane. To simulate axisymmetric deformation, horizontal translation (in the x direction) and meridional rotation were restrained at the apex node of the meridian; to simulate the fixed shell edge, all three freedoms were restrained at the base node of the meridian. A fine FEM mesh was adopted, to ensure that the FEM results were of a high degree of accuracy, thus serving as a benchmark for the analytical results. With elements being ≈0.03 m in length, the mesh had about 500 elements for Case 1 and 770 elements for Case 2.

7.2. Comparison of analytical and FEM results

Both analytical and FEM plots exhibit the characteristic pattern of the edge effect: an oscillating but rapidly decaying stress variation, where after a relatively short distance from the support, the bending disturbance dies out, inner-surface and outer-surface plots merge into one, and the state of stress becomes predominantly membrane. More significantly, analytical and FEM plots closely resemble each other in terms of both their patterns and the magnitude of the stresses. From the close resemblance of the analytical and FEM plots, we may therefore conclude that the proposed analytical formulation gives fairly accurate

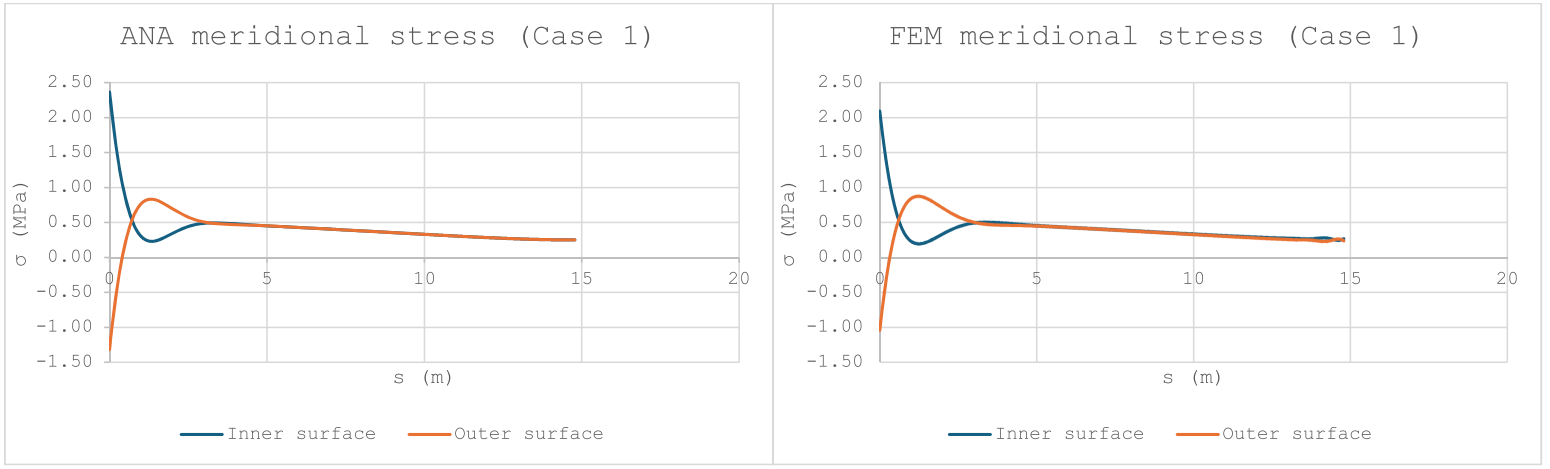

(a)

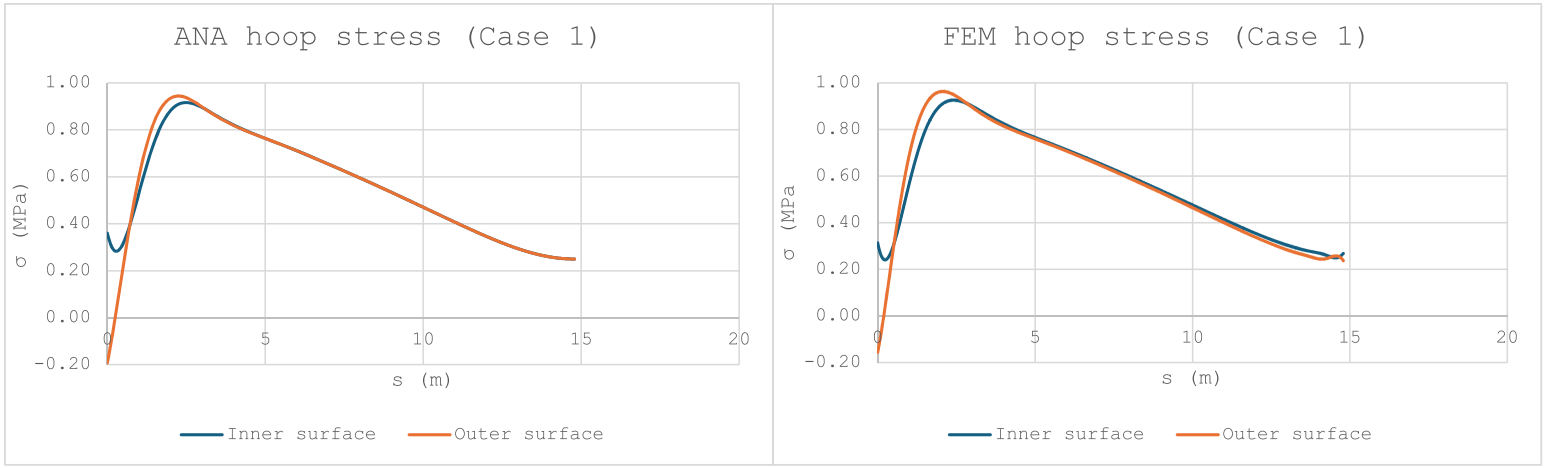

(b)

Fig. 8. Analytical (ANA) versus Finite-Element Method (FEM) stress variations for Case 1 of the parabolic shell of revolution with a fixed edge and subjected to uniform internal pressure: (a) meridional stresses; (b) hoop stresses.

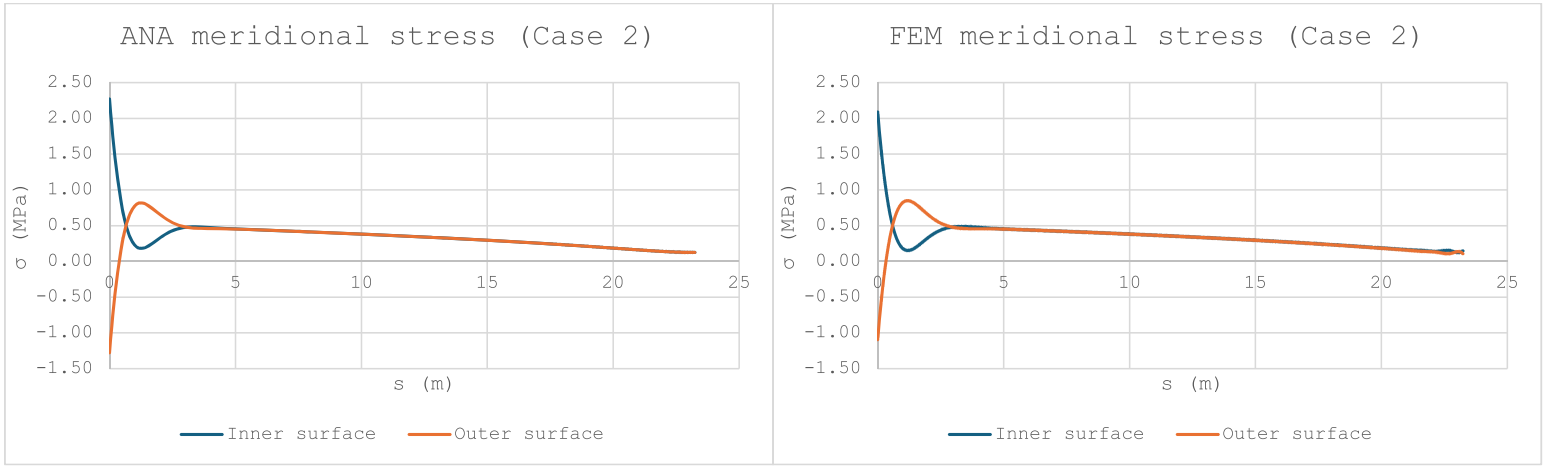

(a)

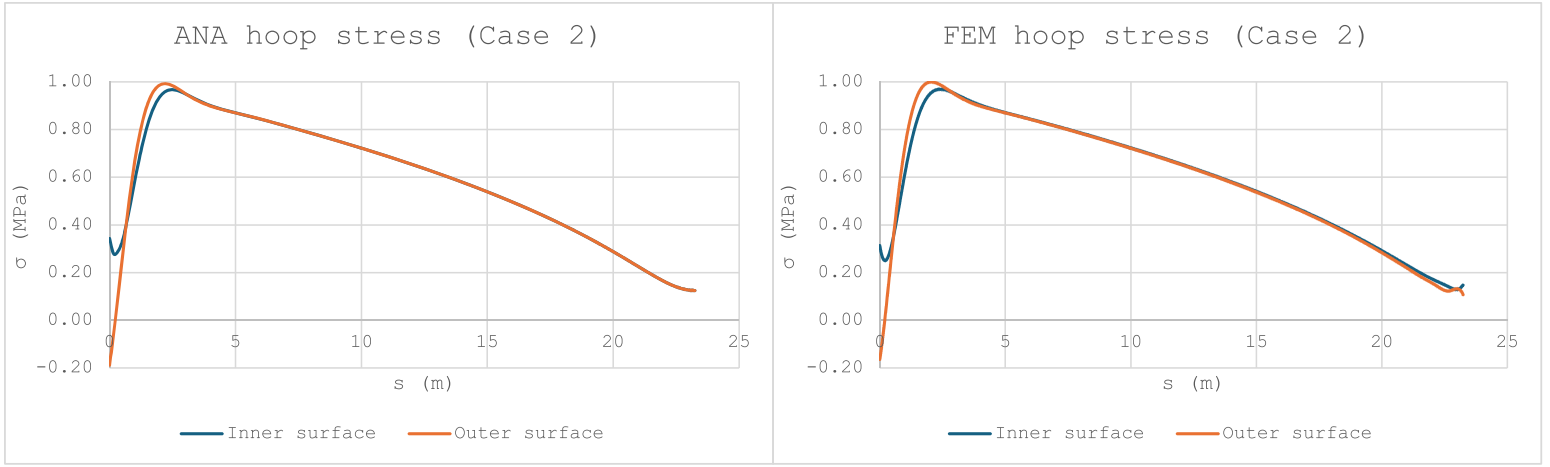

(b)

Fig. 9. Analytical (ANA) versus Finite-Element Method (FEM) stress variations for Case 2 of the parabolic shell of revolution with a fixed edge and subjected to uniform internal pressure: (a) meridional stresses; (b) hoop stresses.

Table 13
Analytical (ANA) versus Finite-Element Method (FEM) stresses for Case 1: Meridional stresses.

Location	Surface	Arc length s (m)	ANA stress (N/mm^2)	FEM stress (N/mm^2)	% diff
support	inner	0	+2.37	+2.09	11.8
	outer	0	−1.32	−1.14	13.6
1st peak	inner	1.30	+0.23	+0.20	13.0
	outer	1.30	+0.83	+0.87	−4.8

Table 14
Analytical (ANA) versus Finite-Element Method (FEM) stresses for Case 1: Hoop stresses.

Location	Surface	Arc length s (m)	ANA stress (N/mm^2)	FEM stress (N/mm^2)	% diff
support	inner	0	+0.36	+0.32	11.1
	outer	0	−0.19	−0.17	10.5
tensile	inner	2.36	+0.92	+0.92	0.0
peak	outer	2.23	+0.94	+0.96	−2.1

Table 15
Analytical (ANA) versus Finite-Element Method (FEM) stresses for Case 2: Meridional stresses.

Location	Surface	Arc length s (m)	ANA stress (N/mm^2)	FEM stress (N/mm^2)	% diff
support	inner	0	+2.27	+2.09	7.9
	outer	0	−1.28	−1.12	12.5
1st peak	inner	1.35	+0.19	+0.17	10.5
	outer	1.35	+0.81	+0.84	−3.7

Table 16
Analytical (ANA) versus Finite-Element Method (FEM) stresses for Case 2: Hoop stresses.

Location	Surface	Arc length s (m)	ANA stress (N/mm^2)	FEM stress (N/mm^2)	% diff
support	inner	0	+0.34	+0.31	8.8
	outer	0	−0.19	−0.17	10.5
tensile	inner	2.46	+0.97	+0.97	0.0
peak	outer	2.12	+0.99	+1.00	−1.0

results.

To obtain a better assessment of the accuracy of the analytical results, stresses at the support location, and at the first turning point of the stress variations, are compared in Tables 13–16. The difference between the peak values of the analytical and FEM results is typically in the range 8 – 14% throughout. This level of agreement is satisfactory, given that only one iteration was performed in the implementation of the proposed approach (refer to Fig. 6), and also given the fact that the Geckeler approximation (upon which the formulation of the bending problem is based) has intrinsic errors of the order of 10% anyway [11]. It is noted that, relative to finite-element modelling, the proposed analytical formulation generally overestimates stresses at the edge of the shell (which errs on the side of safety), the exception being the outer-surface first-peak stresses.

The above results show that the proposed method for accounting for the non-uniform shell slenderness parameter of a polynomial shell of revolution (illustrated here by the parabolic shell of revolution) gives reasonably good estimates of stresses in the edge zone within the limitations of the Geckeler simplification, which itself is an approximate solution approach.

8. Summary and concluding remarks

Even if the thickness parameter does not change appreciably over the edge zone of the shell adjacent to supports, junctions and other discontinuities, non-shallow polynomial shells of revolution of the type $y = kx^n$ (where $n \geq 2$) exhibit a complex bending behaviour in the edge zone, on account of the high rate of change of the meridional radius of curvature (r_1) with respect to the meridional angle ϕ of the shell; the larger the value on n, the higher is this rate of change. This in turn causes the shell slenderness parameter λ to change quite substantially over the edge zone, a behaviour which tends to invalidate approximate methods of analysis such as the Geckeler approximation, as these assume the shell slenderness parameter is constant in the edge zone. Better methods of accounting for the bending behaviour of this class of shells of revolution are required. This has been the motivation for the approach proposed in this paper.

Instead of merely taking an average value of the shell slenderness parameter over the bending-disturbance zone of the shell (which is more of a guess than a well-defined process, since the extent of the bending-disturbance zone is not known until bending effects have been evaluated), a novel and more systematic procedure for determining the effective slenderness parameter λ_e has been proposed in this paper.

Taking the effective extent of the bending disturbance as the location at which the amplitude of the sinusoidal oscillations of the bending disturbance would have decayed to 5% of its initial value (herein referred to as the "inner edge"), and using the Geckeler approximation as the basis for the estimation of the edge effects, the value of the shell slenderness parameter is calculated at the inner edge. The average of the values of the shell slenderness parameter at the outer edge of the bending-disturbance zone (i.e. the physical edge of the shell) and the inner edge (as defined above) gives a first estimate of the effective slenderness parameter λ_e. Using this calculated value of λ_e, a second (and more refined) estimate of the extent of the bending-disturbance zone can be made, leading to a more refined estimate of λ_e. Thus, the proposed method can easily be iterated, if a more accurate estimate of the effective slenderness parameter is required.

Some parametric results for the shell slenderness parameter at the edge of non-shallow parabolic and cubic shells of revolution have been presented; these provide a useful starting point in the bending analysis of such shells. The step-by-step procedure for the calculation of the effective slenderness parameter λ_e has been illustrated by reference to the parabolic shell of revolution, for which some useful parametric results have been tabulated for various values of ρ (depth ratio of the shell) and R/t (shell thinness ratio). The application of the procedure to a real problem has been illustrated by reference to the numerical example of a deep parabolic shell of revolution with a fixed edge (the base of the shell) and subjected to uniform internal pressure, and analytical results for shell stresses compared with those yielded by the finite element method. Despite the fact that only one iteration of the calculation of λ_e was adopted, the agreement was found to be generally close (the difference in peak stresses being typically in the range 8 to 14%).

The overall conclusion is that the proposed approach for the determination of the effective slenderness parameter in non-shallow polynomial shells of revolution gives fairly realistic estimates of shell stresses in the edge zone of the shell, but there is still room for improvement. Further work is being undertaken to try to improve the performance of the basic approach (for example, by taking an average of shell slenderness parameter that is weighted more towards the edge of the shell than the edge of the bending zone, since bending is greatest at the shell edge).

CRediT authorship contribution statement

Alphose Zingoni: Writing – review & editing, Writing – original draft, Methodology, Investigation, Formal analysis, Conceptualization. **Nosakhare Enoma:** Visualization, Validation. **Hlasoa Mahlelebe:** Validation.

Declaration of competing interest

The authors declare that they have no known competing financial interests or personal relationships that could have appeared to influence the work reported in this paper.

Data availability

No data was used for the research described in the article.

References

[1] W. Flügge, Stresses in Shells, Springer, 1973.
[2] S.P. Timoshenko, S. Woinowsky-Krieger, Theory of Plates and Shells, McGraw-Hill, New York, 1959.
[3] V.V. Novozhilov, Thin Shell Theory, Wolters-Noordhoff Publishing, 1970.
[4] A. Zingoni, Shell Structures in Civil and Mechanical Engineering, 1st ed., Thomas Telford Publishing, 1997; 2nd ed., ICE Publishing, 2018.
[5] A.L. Gol'denveizer, Theory of Elastic Thin Shells, Pergamon Press, Oxford, 1961.
[6] A. Zingoni, Stresses and deformations in egg-shaped sludge digesters: discontinuity effects, Eng. Struct. 23 (2001) 1373–1382.
[7] A. Zingoni, Discontinuity effects at cone-cone axisymmetric shell junctions, Thin-Walled Struct. 40 (2002) 877–891.
[8] S.N. Krivoshapko, Research on general and axisymmetric ellipsoidal shells used as domes, pressure vessels and tanks, Appl. Mech. Rev. (ASME) 60 (2007) 336–355.
[9] A. Zingoni, B. Mokhothu, N. Enoma, A theoretical formulation for the stress analysis of multi-segmented spherical shells for high-volume liquid containment, Eng. Struct. 87 (2015) 21–31.
[10] A. Zingoni, N. Enoma, N. Govender, Equatorial bending of an elliptic toroidal shell, Thin-Walled Struct. 96 (2015) 286–294.
[11] A. Zingoni, M.N. Pavlovic, Computation of bending disturbances in axisymmetrically loaded spherical shells: a study of the accuracy of Geckeler's approximation, Eng. Comput. 7 (2) (1990) 125–143.
[12] J. Heyman, Equilibrium of Shell Structures, Clarendon Press, 1977.
[13] M.N. Pavlovic, A. Zingoni, On the elastic design of concrete domes, Struct. Eng. Rev. 6 (1994) 57–69.
[14] A. Zingoni, N. Enoma, Dual-purpose concrete domes: a strategy for the revival of thin concrete shell roofs, Structures 28 (2020) 2686–2703.
[15] A. Zingoni, N. Enoma, On the strength and stability of elliptic toroidal domes, Eng. Struct. 207 (2020) 110241.
[16] A. Zingoni, Self-weight stresses in hyperbolic cooling towers of general shape, Int. J. Space Struct. 14 (1999) 281–294.
[17] A. Zingoni, On membrane solutions for elevated shell-of-revolution tanks of certain meridional profiles, Thin-Walled Struct. 22 (1995) 121–142.
[18] A. Zingoni, Parametric stress distribution in shell-of-revolution sludge digesters of parabolic ogival form, Thin-Walled Struct. 40 (2002) 691–702.
[19] P. Jasion, K. Magnucki, Elastic buckling of clothoidal-spherical shells under external pressure: theoretical study, Thin-Walled Struct. 86 (2015) 18–23.
[20] P. Jasion, K. Magnucki, A pressure vessel with a special barrelled shape, Ocean Eng. 263 (2022) 112414.
[21] A. Zingoni, N. Enoma, Strength and stability of spherical-conical shell assemblies under external hydrostatic pressure, Thin-Walled Struct. 146 (2020) 106472.
[22] W.J. Sutcliffe, Stress analysis of toroidal shells of elliptical cross-section, Int. J. Mech. Sci. 13 (11) (1971) 951–958.
[23] W. Pietraszkiewicz, V. Konopinska, Junctions in shell structures: a review, Thin-Walled Struct. 95 (2015) 310–334.
[24] W. Jiammeepreecha, K. Chaidachatorn, S. Chucheepsakul, Nonlinear static analysis of multi-segmented toroidal shells under external pressure, Thin-Walled Struct. 189 (2023) 110920.
[25] W. Jiammeepreecha, K. Chaidachatorn, K. Klaycham, C. Athisakul, S. Chucheepsakul, Multi-segmented fifth-order polynomial–shaped shells under hydrostatic pressure, Thin-Walled Struct. 203 (2024) 112214.
[26] W. Jiammeepreecha, S. Chucheepsakul, Nonlinear static analysis of an underwater elastic semi-toroidal shell, Thin-Walled Struct. 116 (2017) 12–18.
[27] W. Jiammeepreecha, K. Chaidachatorn, S. Chucheepsakul, Nonlinear static response of an underwater elastic toroidal storage container, Int. J. Solids Struct. 228 (2021) 111134.
[28] W. Jiammeepreecha, K. Chaidachatorn, S. Chucheepsakul, Large displacement analysis of egg-shaped containment shells using Lagrange multipliers, Int. J. Solids Struct. 279 (2023) 112390.
[29] S. Wang, M. Garlock, B. Glisic, Hydrostatic response of deployable hyperbolic-paraboloid umbrellas as coastal armor, J. Struct. Eng. 146 (6) (2020) 04020096.
[30] S. Wang, V. Notario, M. Garlock, B. Glisic, Parameterization of hydrostatic behavior of deployable hypar umbrellas as flood barriers, Thin-Walled Struct. 163 (2021) 107650.
[31] L.A. Godoy, Buckling of vertical oil storage steel tanks: review of static buckling studies, Thin-Walled Struct. 103 (2016) 1–21.
[32] E.M. Sosa, L.A. Godoy, Challenges in the computation of lower-bound buckling loads for tanks under wind pressures, Thin-Walled Struct. 48 (12) (2010) 935–945.
[33] C.A. Burgos, R.C. Jaca, J.L. Lassig, L.A. Godoy, Wind buckling of tanks with conical roof considering shielding by another tank, Thin-Walled Struct. 84 (2014) 226–240.
[34] P. Seide, On the buckling of truncated conical shells under uniform hydrostatic pressure, in: Proceedings of the IUTAM Symposium on the Theory of Thin Elastic Shells, Amsterdam, North-Holland Publishing Company, 1960, pp. 363–388.
[35] J. Singer, Buckling of circular conical shells under axisymmetrical external pressure, J. Mech. Eng. Sci. 3 (1961) 330–339.
[36] B.S. Golzan, H. Showkati, Buckling of thin-walled conical shells under uniform external pressure, Thin-Walled Struct. 46 (2008) 516–529.
[37] T. Von Karman, H.S. Tsien, The buckling of spherical shells by external pressure, J. Aeronaut. Sci. 7 (1939) 43–50.
[38] M. Sato, M.A. Wadee, K. Iiboshi, T. Sekizawa, H. Shima, Buckling patterns of complete spherical shells filled with an elastic medium under external pressure, Int. J. Mech. Sci. 59 (1) (2012) 22–30.
[39] L.H. Sobel, W. Flügge, Stability of toroidal shells under uniform external pressure, Am. Inst. Aeronaut. Astronaut. (AIAA) J. 5 (1967) 425–431.
[40] P.F. Jordan, Buckling of toroidal shells under hydrostatic pressure, Am. Inst. Aeronaut. Astronaut. (AIAA) J. 11 (10) (1973) 1439–1441.
[41] G.D. Galletly, Elastic buckling of complete toroidal shells of elliptical cross-section subjected to uniform internal pressure, Thin-Walled Struct. 30 (1998) 23–34.
[42] A. Combescure, G.D. Galletly, Plastic buckling of complete toroidal shells of elliptical cross-section subjected to internal pressure, Thin-Walled Struct. 34 (1999) 135–146.
[43] D. Redekop, Buckling analysis of an orthotropic elliptical toroidal shell, in: Proceedings of the ASME Pressure Vessels & Piping Conference 3, 2009, pp. 33–40. Design & Analysis.
[44] N. Enoma, A. Zingoni, Buckling of an externally pressurised toroidal shell of revolution with a doubly-symmetric parabolic-ogival cross-section, Int. J. Press. Vessels Pip. 183 (2020) 104106.
[45] N. Enoma, A. Zingoni, Analytical formulation and numerical modelling for multi-shell toroidal pressure vessels, Comput. Struct. 232 (2020) 105811.
[46] P. Jasion, K. Magnucki, Theoretical investigation of the strength and stability of special pseudospherical shells under external pressure, Thin-Walled Struct. 93 (2015) 88–93.
[47] P. Jasion, K. Magnucki, Elastic buckling of Cassini ovaloidal shells under external pressure: theoretical study, Arch. Mech. 67 (2015) 1–14.
[48] K. Sowiński, P. Jasion, Strength and stability of shells based on Booth lemniscate loaded with external pressure, Thin-Walled Struct. 144 (2019) 106284.
[49] J.G. Teng, Buckling of thin shells: recent advances and trends, Appl. Mech. Rev. (ASME) 49 (1996) 263–274.
[50] A. Zingoni, Liquid-containment shells of revolution: a review of recent studies on strength, stability and dynamics, Thin-Walled Struct. 87 (2015) 102–114.